Coordination Chemistry Reviews 417 (2020) 213366

Contents lists available at ScienceDirect

Coordination Chemistry Reviews

journal homepage: www.elsevier.com/locate/ccr

Review

Nano-sized metal-organic frameworks: Synthesis and applications

Xuechao Cai [a,b,1], Zhongxi Xie [a,b,1], Dandan Li [c], Meruyert Kassymova [b], Shuang-Quan Zang [a,*], Hai-Long Jiang [b,*]

[a] College of Chemistry and Molecular Engineering, Zhengzhou University, Zhengzhou 450001, China
[b] Hefei National Laboratory for Physical Sciences at the Microscale, CAS Key Laboratory of Soft Matter Chemistry, Department of Chemistry, University of Science and Technology of China, Hefei, Anhui 230026, PR China
[c] Institutes of Physics Science and Information Technology, Anhui University, Hefei 230601, PR China

ARTICLE INFO

Article history:
Received 25 March 2020
Received in revised form 13 April 2020
Accepted 20 April 2020

Keywords:
Metal-organic frameworks (MOFs)
NanoMOFs
Nanomaterials
Biomedicine
Catalysis
Energy
Membrane separation

ABSTRACT

Recently, nanoscale metal-organic frameworks (nanoMOFs), which leads to the discovery of a variety of properties not observed in their bulk counterparts, have attracted tremendous attention. To be specific, while possessing the properties of bulk MOF materials including high surface area, structural diversity and tailorability etc., nanoMOFs also have some unique advantages, such as accelerated adsorption/desorption kinetics and accessibility to the internal active sites. Moreover, due to their very small sizes and good biocompatibility, nanoMOFs have been widely investigated in biomedicine. In addition, not limited to MOF nanoparticles, their assembly to MOF-based 1-D nanomaterials have also been investigated for catalysis, energy and membrane separation applications. In this review, we first summarize the synthetic strategies of uniform and monodisperse nanoMOFs, and then the intrinsic size-dependent properties towards the most important applications are highlighted as well. Furthermore, the challenges and future prospects of the synthesis and application of nanoMOFs are briefly provided, which we hope will contribute to further push the development of nanoMOF science.

Contents

1. Introduction . . . 2
2. Synthesis of nanoMOFs . . . 2
 2.1. 0-D nanoMOFs . . . 2
  2.1.1. Solvothermal method . . . 2
  2.1.2. Microemulsion method . . . 4
 2.2. NanoMOF-based 1-D materials . . . 6
3. NanoMOFs for biomedical applications . . . 8
 3.1. NanoMOFs for bioimaging . . . 8
 3.2. NanoMOFs for drug delivery . . . 9
 3.3. NanoMOFs as therapeutic agent for cancer . . . 11
4. NanoMOFs for enhanced catalysis . . . 14
5. NanoMOFs for energy . . . 16
6. NanoMOFs for membrane separation . . . 17
7. Conclusions and perspectives . . . 18
 Declaration of Competing Interest . . . 19
 Acknowledgments . . . 19
Appendix A. Supplementary data . . . 19
 References . . . 19

* Corresponding authors.
E-mail addresses: zangsqzg@zzu.edu.cn (S.-Q. Zang), jianglab@ustc.edu.cn (H.-L. Jiang).
[1] These authors contribute equally to this work.

https://doi.org/10.1016/j.ccr.2020.213366
0010-8545/

1. Introduction

Nanomaterials refer to materials with at least one dimension at the nanometer size (1–100 nm) or composed of them as basic units in three-dimensional space and have gained great attention since their emergence [1]. The small-size particles give nanomaterials some unique properties different from those of bulk counterparts. Take their application in the field of catalysis as an example, the nano-sized crystals usually show a better exposure of catalytic sites because of their larger surface area. In addition, the shorter diffusion distances in the nanocrystals facilitate the interaction between substrates and catalytic centers, thus nano-sized catalysts usually possess better catalytic activity than their bulk analogues [2]. Moreover, nanomaterials with small size effect, quantum size effect, macroscopic quantum tunneling effect, etc., can lead to the relatively new acoustic, optical, electrical, magnetic and thermal properties. They have been widely used in the fields such as nano electronic devices, medicine and health, aerospace, aviation and space exploration, environment, resources and energy, biotechnology, etc. From different angles of perspectives toward diverse ends, the benefits of this "miniaturization" are very amazing [3].

Metal-organic frameworks (MOFs), a new class of porous hybrid materials formed by the self-assembly of metal ions/clusters and organic ligands, have captured great attention and achieved tremendous developments in the last twenty years [4–14]. Due to their unique characteristics such as high surface area, structural diversity and tailorability, etc., MOF materials offer prospective applications in catalysis [15–28], gas storage and separation [29–36], biomedicine [37–45], chemical sensing [46–54], energy applications [55–62] and many other fields [63–66]. Very recently, much attention has started to explore the synthesis and applications of nanoscale MOFs (nanoMOFs), the particles of which feature at least one dimension at the nanoscale. So far, nanoMOFs have shown particular advantages compared to their bulk materials with unique properties, such as accelerated adsorption/desorption kinetics and accessibility to the internal active sites for enhanced catalysis, suitable sizes for biomedical application, and their assembly to diverse nanostructured materials for energy and membrane separation-related applications, etc.

Considering that there have been several excellent review articles on the nano-/micro-scaled MOF materials [67–72], herein we would mainly update the latest and most important research results about nanoMOFs with uniform size and good monodispersity as well as the MOF-based 1-D nanomaterials. Especially, we will emphasize the importance of "general strategy", as this is more conducive to the practical application of nanoMOFs. In this review article, we will mainly introduce MOF nanoparticles, that is, zero-dimensional (0-D) nanoMOFs. Then we will discuss their applications in nanomedicine, catalysis, energy and membrane separation. In addition, we also discuss the synthesis of some nanoMOF-based one-dimensional (1-D) materials that are almost generated through the self-assembly of 0-D small particles based on templates. For the two-dimensional (2-D) MOFs, i.e. MOF nanosheets, although they are also nanoscale in one of their dimensions, considering the existence of some excellent reviews recently [68,73–75], will not be discussed here. Our purpose is to arouse more researchers' attention to the application of nanoMOF materials and thus further promoting the development of nanoMOF science in more fields.

2. Synthesis of nanoMOFs

2.1. 0-D nanoMOFs

In recent years, although quite a few synthetic methodologies have been exploited for preparing nanoMOF materials, the general synthesis of uniform and monodisperse nanoMOF particles, i.e. 0-D nanoMOFs, still remains significant challenge. On the basis of classical crystallization mechanism, segregating the nucleation and growth is critical process to obtain uniform nanocrystals [76]. The credible synthesis of nanoMOFs depends on an understanding of the initiation, growth, and termination process of the nanocrystals. Previously, the LaMer model has been used to explain the growth process of MOF crystals [77]. This model separates crystal nucleation from growth and reveals that high concentration of precursor can trigger thermodynamic driving forces. Based on this empirical law, general synthetic strategies of uniform nanoMOFs with good monodispersity mainly include solvothermal and microemulsion methods. It is worth noting that, although ultrasound and microwave methods have also been reported for preparing nanoMOFs, the homogeneity and monodispersity of nanoMOFs are usually difficult to guarantee, so we would not discuss the preparation of nanoMOF materials by these methods. In this part, we will only focus on recent significant advances for fabricating nanoMOFs with uniform morphology and good monodispersity.

2.1.1. Solvothermal method

Solvothermal strategies are the most effective and universal strategies for preparing nanoMOFs thus far. In the initial period, the foremost arguments such as stoichiometric ratio, reaction time, pH and temperature are focused to regulate the size of MOF crystals [78]. Although some nanoMOFs (e.g. Fe-MIL-88A [79], MIL = Materials of "Institut" Lavoisier; Fe-MIL-89 [80]; MOF-5 [81]; ZIF-8 [82]; ZIF = Zeolitic Imidazolate Framework) and ZIF-90 [83] can be synthesized by accurately regulating the above parameters, this process is usually difficult to be well controlled, leading to the agglomeration of nanoMOFs because of the higher surface energy. To deal with this problem, Kitagawa and co-workers introduced chemical modulators into the synthetic process to optimize the morphology and size of nanoMOFs (Fig. 1) [84]. In the process of nucleation and growth of MOF nanocrystals, modulators are usually able to compete with organic connectors that cooperate with metal ions. As a result, the reaction rate, crystalline morphology and size were precisely regulated. In their study, when different amounts of acetic acid were added during the synthesis of $[Cu_2(ndc)_2(dabco)_n]$ (ndc = 1,4-Naphthalenedicarboxylic acid; dabco = 1,4-diazabicyclo[2.2.2]octane), nanoparticles with a size of 5 nm, nanocubes with an average size of 80 nm, and nanorods with diameters of around 80 nm were obtained. Different from the previous solvothermal method, modulators were used to adjust the coordination interaction of organic linkers and metal ions.

It should be noted that modulators can play different roles in regulating particle size of MOFs. In some cases, modulators can slow down the crystal growth of MOFs, leading to the formation of smaller MOF crystals; in other cases, larger crystals are obtained by slowing down the rate of nucleation. The final results can be controlled by the coordination strength between metal ions/clusters and modulators as well as the concentration of the modulators [77]. Meanwhile, the modulators can also regulate the morphology of MOFs. Hence, diverse modulators such as acetic acid, benzoic acid and lauric acid, etc., are widely used to regulate the particle size, monodispersity and uniformity of nanoMOFs.

Recently, Wang and co-workers developed a universal synthetic method towards nanosized Zr-, Hf-based MOFs by regulating the hydrolysis rate of metal salts in water, meanwhile the acetic acid was introduced as a regulator to regulate the coordination environment [85]. Take the synthesis of UiO-66-NH_2 (UiO = Universitetet i Oslo) as an example, when the concentration of H_2O and acetic acid were precisely controlled, uniform MOF nanoparticles with an average size of 200 nm were prepared within 15 min. Further control experiments were performed to acquire the synthetic mechanism of the uniform Zr-MOF nanocrystals. The concentration of

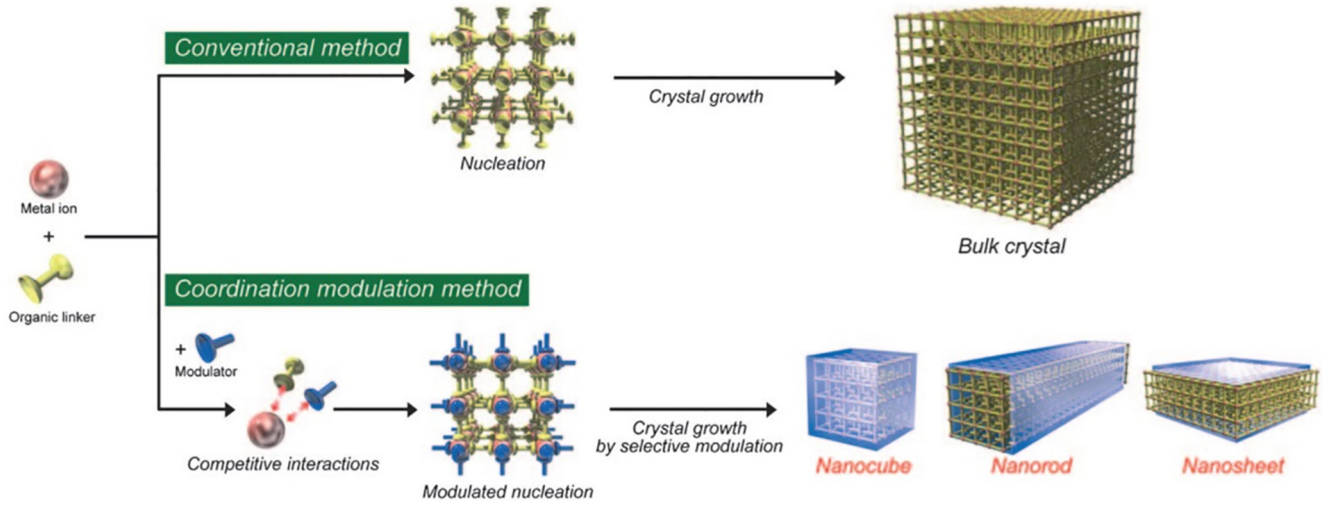

Fig. 1. The role of chemical modulators for fabricating MOF nanocrystals. Reproduced from ref. 84 with permission from Wiley-VCH, copyright 2009.

acetic acid and H_2O was found to play an important role. Acetic acid was used as modulator to adjust the coordinated environment between metal ions and ligands. Time dependent electrospray ionization-mass spectrometry (ESI-MS) measurements were employed to prove that the water can accelerate hydrolysis during the synthetic process. As a result, the presence of H_2O and acetic acid jointly induced the formation of uniform MOF nanoparticles. It is interesting to find that this method can be extended to synthesize other types of Zr-MOFs, including UiO-66, UiO-66-$(OH)_2$, UiO-66-2,6-NDC, UiO-67, BUT-12 and PCN-222-Co. More importantly, this synthetic strategy is effective to prepare Zr-, Hf-based nanoMOFs at the gram-scale, which shows bright potential in the industrial application of nanoMOFs.

In the preparation of MOF materials, polymers and/or surfactants are usually used to control the particle growth and/or shape, and they sometimes go into the skeleton of the MOFs and become part of the MOF materials. For instance, the common polymers such as polyethylene glycol (PEG) and polyvinylpyrrolidone (PVP) can modulate the size, uniformity and monodispersity of MOF materials [86–90]. Recently, Johnson and coworkers reported the preparation of nano-sized polyMOFs. In this work, different from the order of adding coordination modulators in previous examples, organic linkers were first coupled with a polymer, i.e. PEG methyl ether azide (Fig. 2a) [91]. Interestingly, the length of polymer chains can distinctly affect the size and the size decreases as the molecular weight increases. Take synthetic polyMOF-5 as an example, the smaller nanoparticles with a diameter of about 28 nm were synthesized via a solvothermal method by mixing PEG5k-L_4, terephthalic acid, and $Zn(NO_3)_2{\cdot}6H_2O$ in N,N-Dimethylformamide (DMF) (Fig. 2b). The size of the obtained MOF-5 nanoparticles is less than 30 nm. When the polymer PEG10k-L_4, a substitute whose molecular weight is larger than that of PEG5k-L_4, was used during the synthesis, the smaller nanoparticles (20 ± 1 nm) were formed (Fig. 2c). Delightedly, thanks to the universal multivalent effect of this approach, it can be extended to prepare other MOFs. The well-defined polyUiO-66 nanoparticles with the diameter of 36 ± 4 nm were synthesized by using PEG10k-L_4 (Fig. 2d, e).

With further understanding of the synthetic mechanism of nanoMOFs, some methods are established to command the size of nanoMOFs according to the precise separation of nucleation and growth process. Recently, Wang and co-workers developed a universal method by accurately adjusting the size of nanoMOFs by separating the nucleation and growth process [92]. In this method, a spot of metal ions were pre-added to the solutions containing organic ligands. After a part of clusters linked by metal node and organic ligand were formed, the total metal ions were introduced and the seeds could grow into large crystals (Fig. 3a). By changing the molar ratio between pre-added Zn^{2+} and organic ligands, the size of ZIF-8, ZnCo-BMOF and nanopaticles@ZIF-8 can be adjusted. Further experimental data reveal that the size of the nanoparticles decreases as the molar ratio increases (Fig. 3b).

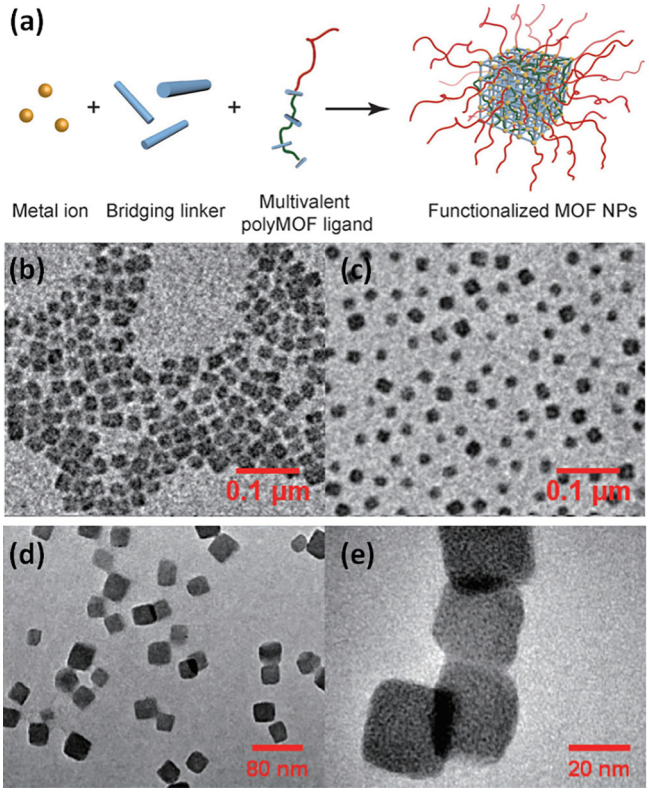

Fig. 2. (a) Formation mechanism of nano polyMOFs by using multivalent ligands as modulators. (b) TEM image of polyMOF-5 nanoparticles of 28 ± 2 nm in diameter synthesized by using PEG5k-L_4. (c) TEM image of polyMOF-5 nanoparticles of 20 ± 1 nm in diameter synthesized by using PEG10k-L_4. (d, e) TEM image of polyUiO-66 nanoparticles of 36 ± 4 nm in diameter synthesized by using PEG10k-L_4. Reproduced from ref. 91 with permission from Wiley-VCH, copyright 2019.

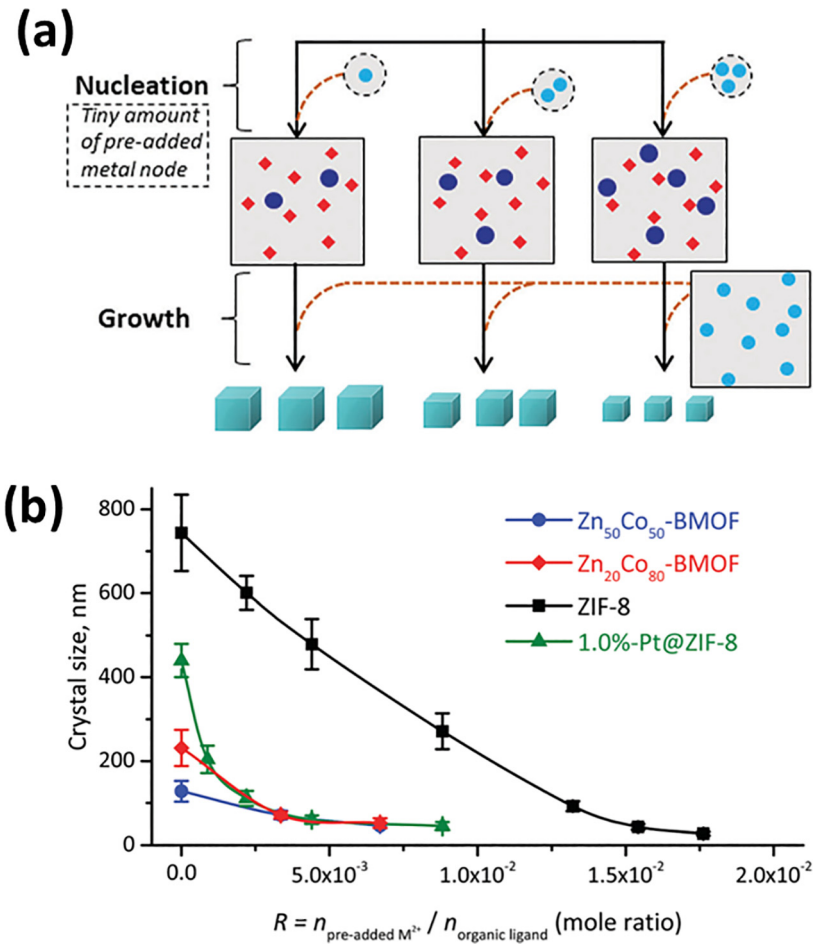

Fig. 3. (a) Formation mechanism for the nucleation and growth separated method. (b) Dependence of the particle size on the molar ratio of the pre-added Zn^{2+}/organic ligand. Reproduced from ref. 92 with permission from Royal Society of Chemistry, copyright 2018.

Very recently, Zhang and co-workers developed a very effective and universal strategy to precisely synthesize a series of nanoMOFs by separating the nucleation and growth process [93]. The metal ions and ligand solution were added to the stirring reaction system at a controlled feed rate by an injection pump. The purpose of this operation is to regulate the degree of supersaturation during the reactions. As the reaction proceeds, there is a dynamic equilibrium between the consumption of the reactants and the generation of the products. On the basis of LaMer diagram (Fig. 4a), the supersaturation degree increases quickly when reagents enter the reaction system continuously. Because the process of nuclei growth leads to the quick consumption of reactants, the supersaturation degree will decline quickly, resulting in the end of nucleation. Afterwards, continuous addition of reactants can ensure the growth of the nanocrystals. Take the preparation of HKUST-1 as an example, a faster feed rate in the process of nucleation will increase the amounts of the generated nucleis, so the size of products is smaller than that of a slower feed rate. Because the nucleation and growth process are separated via adjusting the concentration of reactants, the product can grow continuously without agglomeration when reactants are sufficient (Fig. 4b). Moreover, this synthetic method can be extended to synthesize more kinds of nanoMOFs, including MIL-101(Fe), MOF-801, MIL-100(Fe), ZIF-67, ZIF-8 and UiO-66-(Zr), making this method more general and practical.

2.1.2. Microemulsion method

Microemulsion synthesis is effective for preparing uniform and monodispersed nanoMOFs. In this synthetic system, the microemulsion is usually formed by incompatible solvents under the action of emulsifiers or surfactants and they are almost monodisperse systems and thermodynamically stable [94]. Monodispersed nano-droplets can form in the process of mixing and size of droplets can be regulated by adjusting the concentration of surfactants. Mann and coworkers reported the preparation of highly monodispersed Prussian Blue nanoparticles by this method [95]. Whereafter, Lin and co-workers have performed lots of explorations on the preparation of nanoMOFs by using this technique. They synthesized crystallographic $Gd_2(BDC)_{1.5}(H_2O)_2$ nanorods with $GdCl_3$ and bis(methylammonium)benzene-1,4-dicarboxylate in a micro-emulsion system that is composed of hexadecyl trimethyl ammonium bromide (CTAB)/water/isooctane/1-hexanol [96]. The nanoMOFs can be downsized from 2 μm × 100 nm to 125 nm × 40 nm when changing the ratio of water to CTAB from 10:1 to 5:1. This demonstrates that the aspect ratios of MOF increase with the ratio of water to surfactant. In addition, the average size of particles decreases with the increase of the reactant concentration, which may because the micelles containing the reactant increase, causing more nucleation sites, resulting in a decrease in particle size. Similarly, this reverse-phase microemulsion can be extended to synthesize $[Gd(BTC)(H_2O)_3]\cdot H_2O$ and $Mn_3(BTC)_2(H_2O)_6$ [97].

Very recently, Cai et al. prepared highly uniform HKUST-1 nanocrystals via a reverse-phase microemulsion method [98]. First, a micro-emulsion system was constructed by adding sodium hydroxide solution, oleic acid (OA) and n-hexane into ethanol solution. After introducing divalent copper ions into the

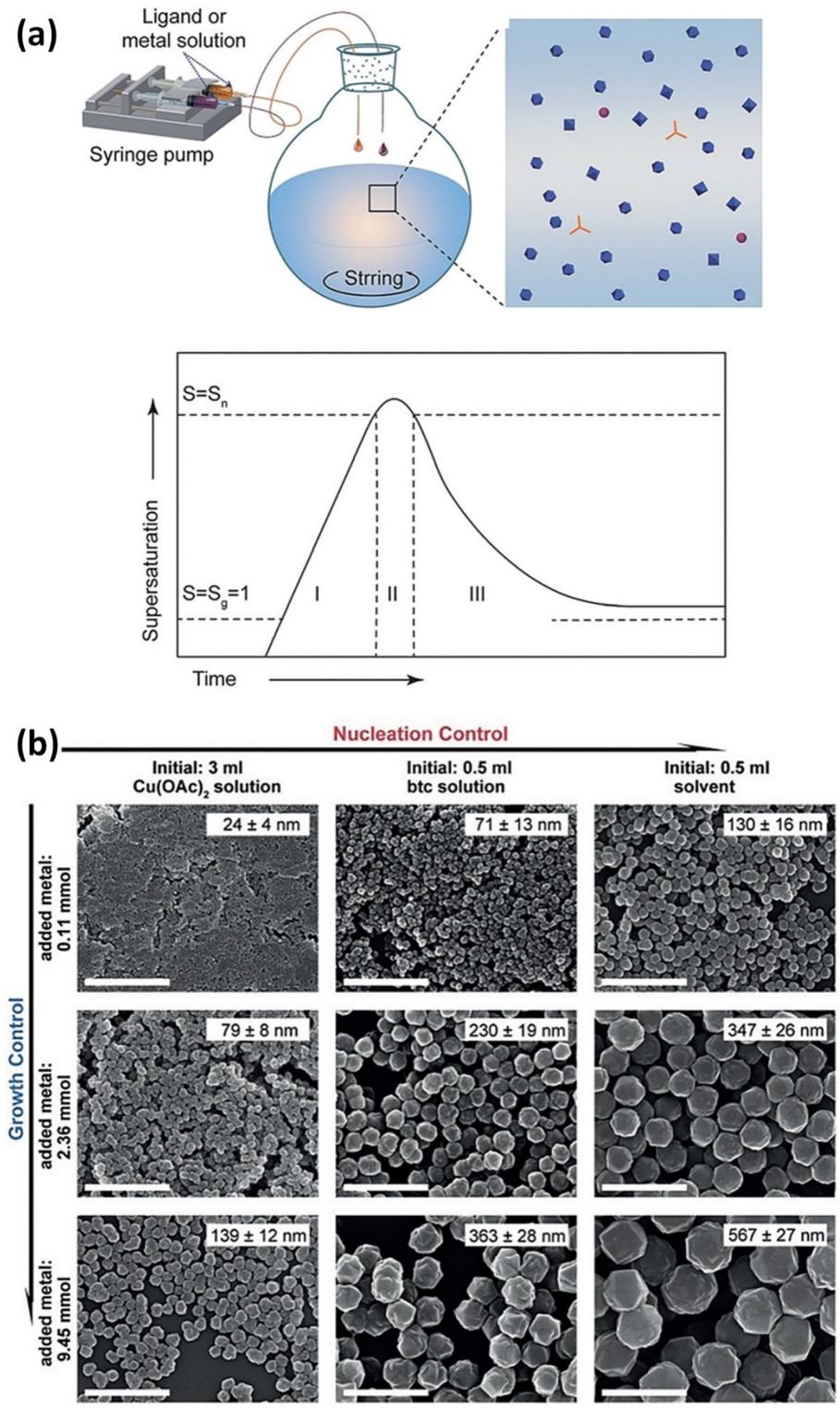

Fig. 4. (a) Schematic illustration of the synthetic process and mechanism of nanoMOFs. (b) SEM images of HKUST-1 nanoparticles prepared by different initial solutions after adding different monomers (added metal/ligand = 3/2). Scale bar is 1 μm. Reproduced from ref. 93 with permission from Wiley-VCH, copyright 2018.

mixture, copper oleate clusters were formed, followed by the reaction with 1,3,5-benzenetricarboxylic acid (BTC) ligands. Finally, HKUST-1 nanocrystals formed gradually and were "protected" by OA (Fig. 5a). Interestingly, the crystal size can be adjusted by the amount of surfactant, i.e. OA, in this report. When the amount of OA was increased from 0.20 to 0.40 mL, while holding the other parameters invariant, the sizes of the HKUST-1 increased from 30 to 140 nm. Particularly, when 0.30 mL of OA was used, uniform HKUST-1 nanospheres with an average particle size of around 70 nm were prepared (Fig. 5b-e). In addition, an iron(III)-based nanoMOF was also prepared by this method [99,100].

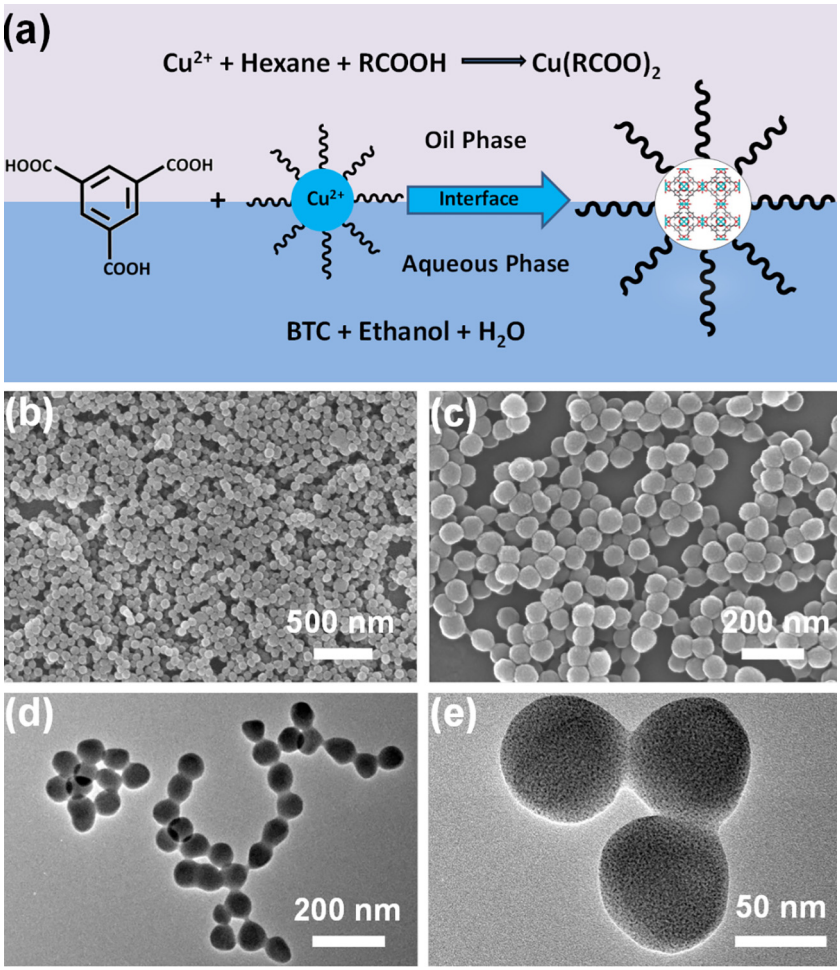

Fig. 5. (a) Schematic diagram of synthetic mechanism of HKUST-1 nanocrystals. SEM (b, c) and TEM (d, e) images of nano HKUST-1 with different magnifications. Reproduced from ref. 98 with permission from the American Chemical Society, copyright 2019.

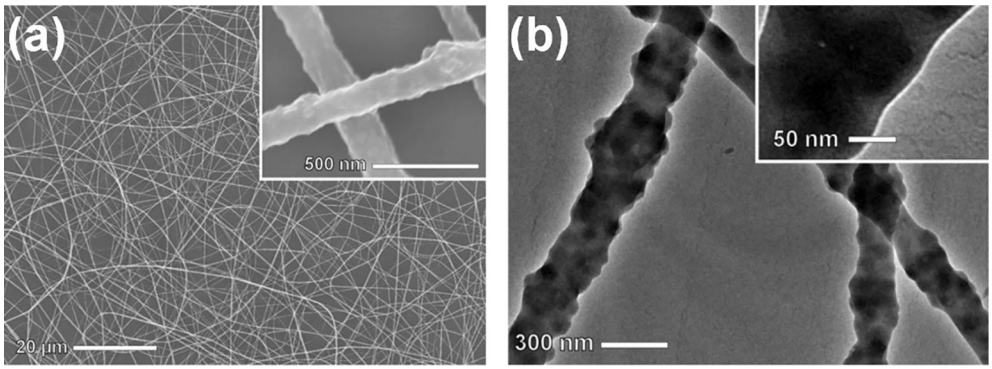

Fig. 6. (a) SEM and (b) TEM images of ZIF-8 nanoparticles in polyvinylpyrrolidone (PVP). Adapted from ref. 105 with permission from Royal Society of Chemistry, copyright 2011.

2.2. NanoMOF-based 1-D materials

The 1-D MOF materials have received great concern in recent years [101–104]. Among them, nanoMOF-based 1-D materials are mostly produced by the self-assembly of 0-D MOF nanoparticles by using 1-D templates. Ostermann et al. prepared highly porous 1-D nanofibers by electrospinning ZIF-8 nanoparticles with PVP (Fig. 6). The colloidal suspensions of nanosized ZIF-8 particles were first prepared and separated by centrifugation, and then the obtained ZIF-8 nanoparticles were re-dispersed in methanol and concentrated to 3.5–4.5 wt% by vacuum distillation. For the following electrospinning process, the PVP methanol solution was added to the colloidal ZIF-8 nanoparticles and stirred thoroughly. Finally, the solution was injected by a syringe pump through a metal needle. Due to the good affinity with PVP molecules, ZIF-8 nanoparticles can be evenly dispersed into the nanofibers. Finally, the size of

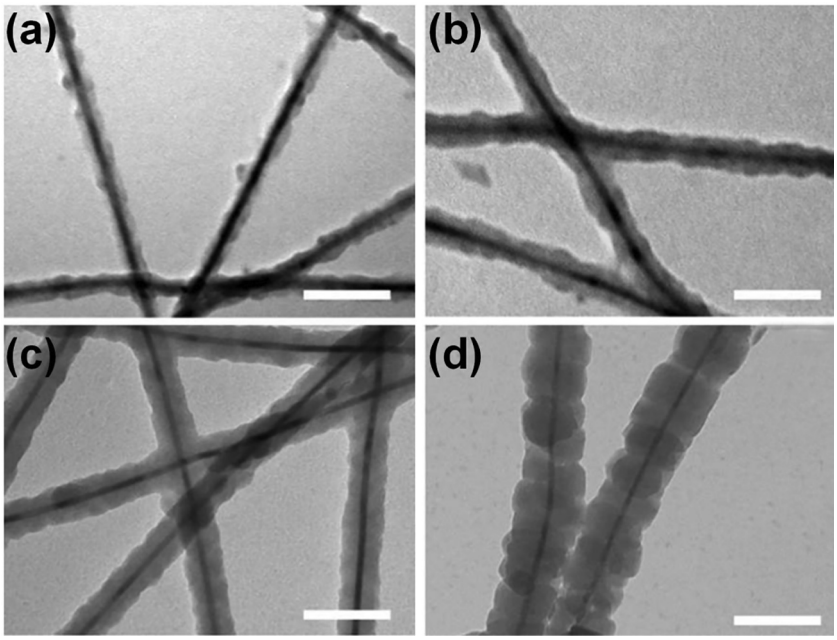

Fig. 7. (a)-(d) TEM images of as-obtained Te@ZIF-8 nanofibers via changing the contents of precursors. The average diameter from (a) to (d) is 27, 36, 45 and 73 nm, respectively. Scale bar is 100 nm. Adapted from ref. 106 with permission from the American Chemical Society, copyright 2014.

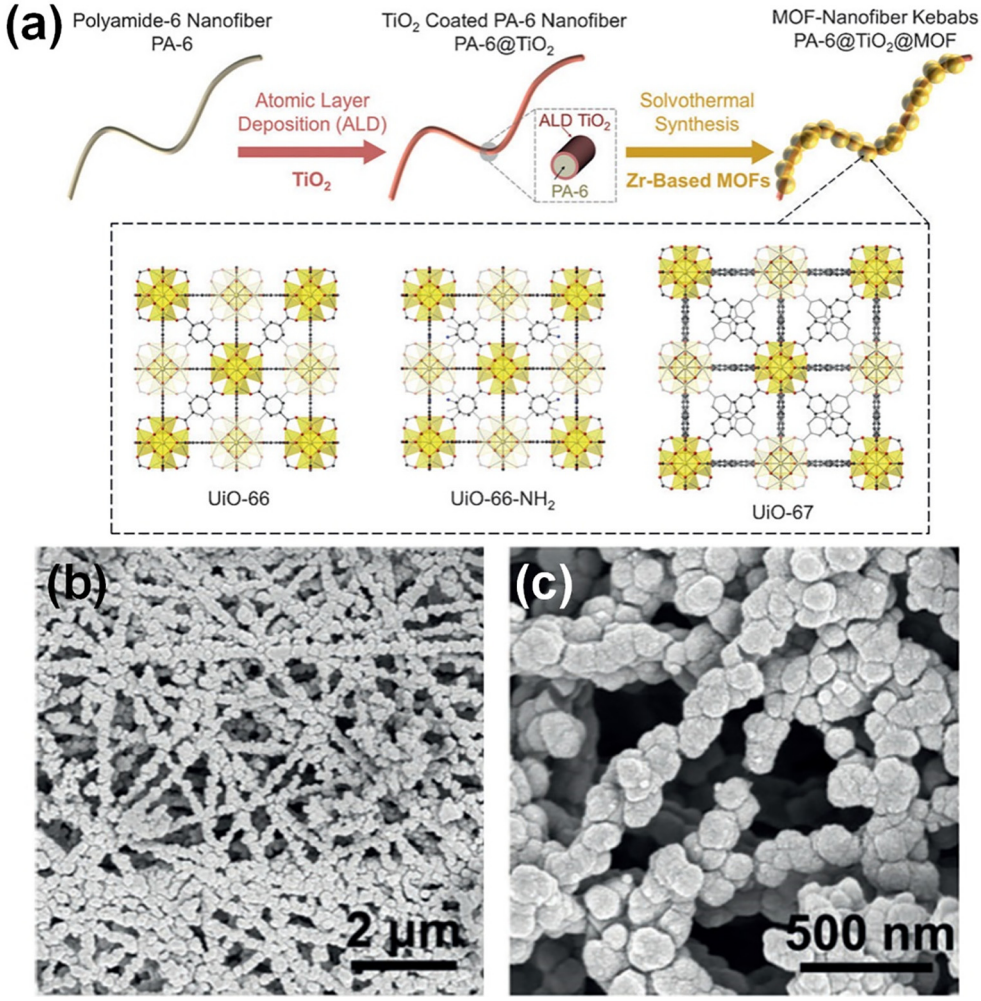

Fig. 8. (a) Schematic illustration for Zr-based MOF nanofibers on polyamide-6. (b-c) SEM images of PA-6@TiO_2@UiO-66-NH_2. Adapted from ref. 109 with permission from Wiley-VCH, copyright 2016.

the nanofibers was 150–300 nm, and could be adjusted by changing the amount of PVP. The obtained MOF-polymer nanofibers combined the advantages of both materials [105].

Yu and coworkers reported the nanowire-directed templating synthesis of 1-D nanoMOFs [106]. The ultrathin tellurium nanowires (TeNWs) with great dispersibility were first prepared by a hydrothermal method. Thanks to the precursor of ZIF-8 tends to adhere to the active surface of TeNWs, ZIF-8 nanoparticles can spontaneously and uniformly grow onto the TeNWs to construct 1-D nanofibrous structures by a freeze-drying technique. Moreover, by varying the amounts of precursor, the size of ZIF-8 nanofibers can be precisely adjusted from 27 to 73 nm, respectively (Fig. 7). Finally, the uniform Te@ZIF-8 nanofibers with high aspect ratio and steerable sizes were obtained. Recently, Yu's group continued to fabricate the 1-D MOF nanofibers that were by self-assembly of bimetallic ZIF nanoparticles (BMZIFs) [107]. The nano-sized BMZIFs were first prepared in methanol and the synthetic process was analogous to that of ZIF-8 by doping $Co(NO_3)_2 \cdot 6H_2O$ with different molar proportions [108]. Then a kind of polymer, polyacrylamide (PAN), was employed as the template of electrospun fibers. The as-prepared BMZIFs were mixed with PAN in DMF to produce an electrospinning stock solution. Followed by the electrospinning technique, a series of uniform BMZIFs/PAN fibers with the 1-D structure were successfully prepared.

Parsons and coworkers prepared a series of MOF-nanofiber composites [109]. As shown in Fig. 8a, the standalone polyamide-6 nanofibers prepared by electrospinning were first covered by a thin-layer of TiO_2 to facilitate MOF heterogeneous nucleation on the fibers. Then UiO-66, UiO-66-NH_2 and UiO-67 were coated on the above prepared fibers, respectively. Specifically, the TiO_2-coated PA-6 nanofiber was added during the synthesis of the MOFs and maintained at 85 °C for 24 h. At the end of the solvothermal synthesis, the MOF nanofibers were collected. SEM images (Fig. 8b, c) showed that UiO-66-NH_2 nanocrystals with average sizes of 126 ± 25 nm were arranged closely on the polyamide-6@TiO_2 nanofibers.

In another recent work, the magnetic MOF nanofibers were prepared [110]. Specifically, inorganic hydroxyapatite (HAP) nanowires were first modified with Fe_3O_4 nanoparticles on the surface. Then the magnetic MOF nanofibers were prepared by self-assembly of Fe-MIL-100 nanocrystals via a layer-by-layer method. The surface of hydroxyapatite nanowires possesses lots of functional groups, which can promote the following deposition of the magnetic nanoparticles and Fe-MIL-100 nanocrystals. Finally, TEM images showed that a uniform layer of MOF (ca. 50 nm) was coated on the magnetic HAP nanowires.

3. NanoMOFs for biomedical applications

Due to their suitable sizes, chemical versatility, good biocompatibility, tunable structure, appropriate and physiological stability, etc., nanoMOFs have been extensively used in biomedical applications during the last ten years [37–43,111,112]. In the early time, nanoMOFs are mainly focused on drug delivery and bioimaging [37,111–118]. As the nanoMOF science continues, more functional nanoMOFs are developed for medicine applications. For example, the porphyrin or porphyrin derivatives-based nanoMOFs are very competitive in photodynamic therapy (PDT) of cancers, which can overcome the self-aggregation of porphyrin molecules in physiological conditions [119–127]. Although the nanoMOFs for biomedical applications are still in the preclinical stage, some Fe, Zn and Cu-based nanoMOFs have shown good prospects due to their low toxicity and high therapeutic effect. We hope new development for future study in the use of nanoMOFs for clinical applications.

3.1. NanoMOFs for bioimaging

As an emerging imaging probe, nanoMOFs have been broadly studied for bio-imaging [128]. These materials are good candidates for imaging contrast agents due to their different compositions and structures. Especially, some Gd^{3+}-, Mn^{2+}- and Fe^{3+}-containing nanoMOFs have presented great efficiency for magnetic resonance imaging (MRI), which is a non-invasive imaging technology that detects the direction of nuclear spin in a magnetic field. Lin and colleagues demonstrated that the $Gd(BDC)_{1.5}(H_2O)_2$ nanorod with size of about 100 nm in length and 40 nm in diameter could act as both T_1 and T_2-weighted contrast agents, which had a longitudinal relaxivity (R_1) value of 35.8 s^{-1} and a transverse relaxivity (R_2) of 55.6 s^{-1} per mM of Gd^{3+}, respectively. More importantly, the r_1 value of this nanoMOF was higher than that of Omniscan, a kind of contrast agent for clinical use [96] (Fig. 9). Since this early-stage report, many other Gd-based nanoMOFs were investigated to exhibit extremely high MR relaxivities [129–134], demonstrating that MOFs can act as splendid MRI agents.

Due to the relatively large biological toxicity of Gd ions [135], Mn^{2+}-based nanoMOF T_1-weighted contrast agents have gradually developed because of the lower toxicity of Mn^{2+} than that of Gd^{3+} [136]. Lin and coworkers prepared nanorod-like $Mn(BDC)(H_2O)_2$ and nanoblock-like $Mn_3(BTC)_2(H_2O)_6$ for T_1-weighted contrast agents. After surface functionalization with a thin layer of silica and a cell-targeting molecule, in vivo MR imaging in spleen and liver was accomplished [97]. Afterwards, some Mn^{2+}-containting nanoscale coordination polymers (NCPs) were also reported to act as enhanced T_1-weighted contrast [137,138]. Recently, a porous

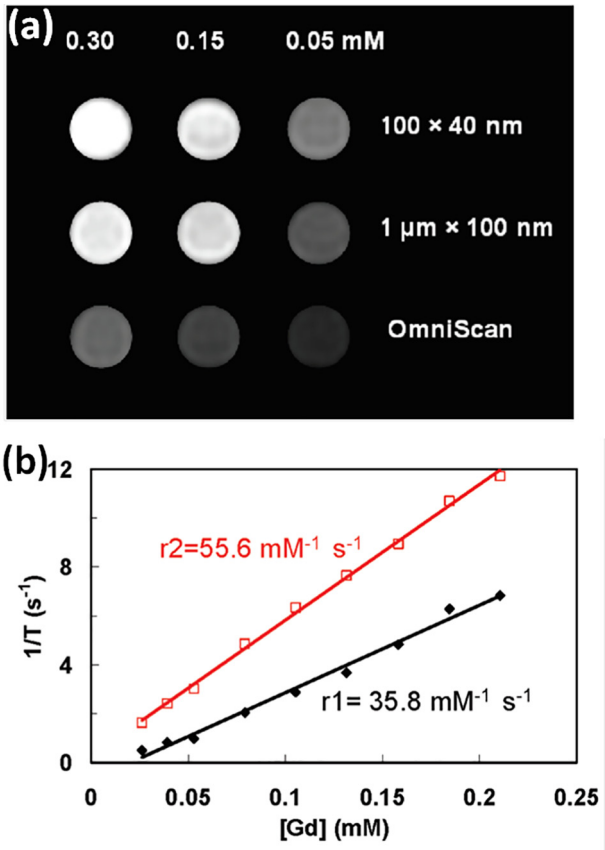

Fig. 9. (a) T_1-weighted MR images of nano $Gd(BDC)_{1.5}(H_2O)_2$ in 0.1% xanthan gum aqueous solution. (b) R_1 and R_2 relaxivity curves of nano $Gd(BDC)_{1.5}(H_2O)_2$ with size of 100 nm × 40 nm. Reproduced from ref. 96 with permission of American Chemical Society, copyright 2006.

Mn-porphyrin-based nanoMOF (PCN-222(Mn)) was constructed. Due to the high dispersibility of Mn^{3+} in the framework and the hydrophilia channel, this nanoMOF worked as T_1-weighted contrast and exhibited a high r_1 relaxivity of ~35.3 mM^{-1} s^{-1} at 1.0 T [139].

Different from Gd^{3+} and Mn^{2+}-based nanoMOFs, Fe^{3+}-based MOFs usually lead to negative image enhancement. Horcajada and cooperators prepared a series of non-toxic iron(III) carboxylate nanoMOFs as T_2-weighted contrast agents [116]. After modifying PEG on its surface, the nanoMIL-88A showed high r_2 relaxivity with 95 mM^{-1} s^{-1} and it showed obviously negative enhancement in the spleen and liver of Wistar rats after injection by 30 min (Fig. 10). More meaningfully, mouse metabolism experiments showed that the PEG-nanoMIL-88A can be completely excluded in three months, which provides great potential for future clinical applications of this nanoMOF.

Some nanoMOFs containing high-Z number elements can be used as X-ray computed tomography (CT) imaging based on X-ray sample attenuation, which can provide 3D images with good spatial resolution [140]. deKrafft et al. reported the construction of I_4-BDC with Cu^{2+} and Zn^{2+}. Based on the containing iodine element, the two nanoMOFs were used for CT imaging and showed better imaging results than the commercial contrast agent iodixanol [141]. In addition, two kinds of nanoMOFs with UiO-66 structure containing high contents of Zr (37 wt%) and Hf (57 wt%) were synthesized. Especially, due to the higher attenuation of Hf than Zr, the nano Hf-based MOF functionalized by silica and PEG exhibited high performance as CT contrast agent for spleen (131 HU) or liver (86 HU) imaging [142].

3.2. NanoMOFs for drug delivery

The drug carrier refers to a system that can change the way the drug enters the body and its distribution in the body, control the release rate of the drug, and deliver the drug to the target organ. Drug carrier materials play a very important role in the research of controlled-release carriers. Among the commonly used nano-drug carriers, such as polymers, lipids, silicon materials, carbon structures, inorganic oxides and carbides, etc., MOF materials are excellent candidates to deliver small molecule drugs due to their good biological safety and inherently porous nature. In addition, the biggest advantage of MOFs as drug carrier is not only the high drug loading, but also the long drug release time. In the earlier period, nanoMOFs often acted as carriers for some common anticancer

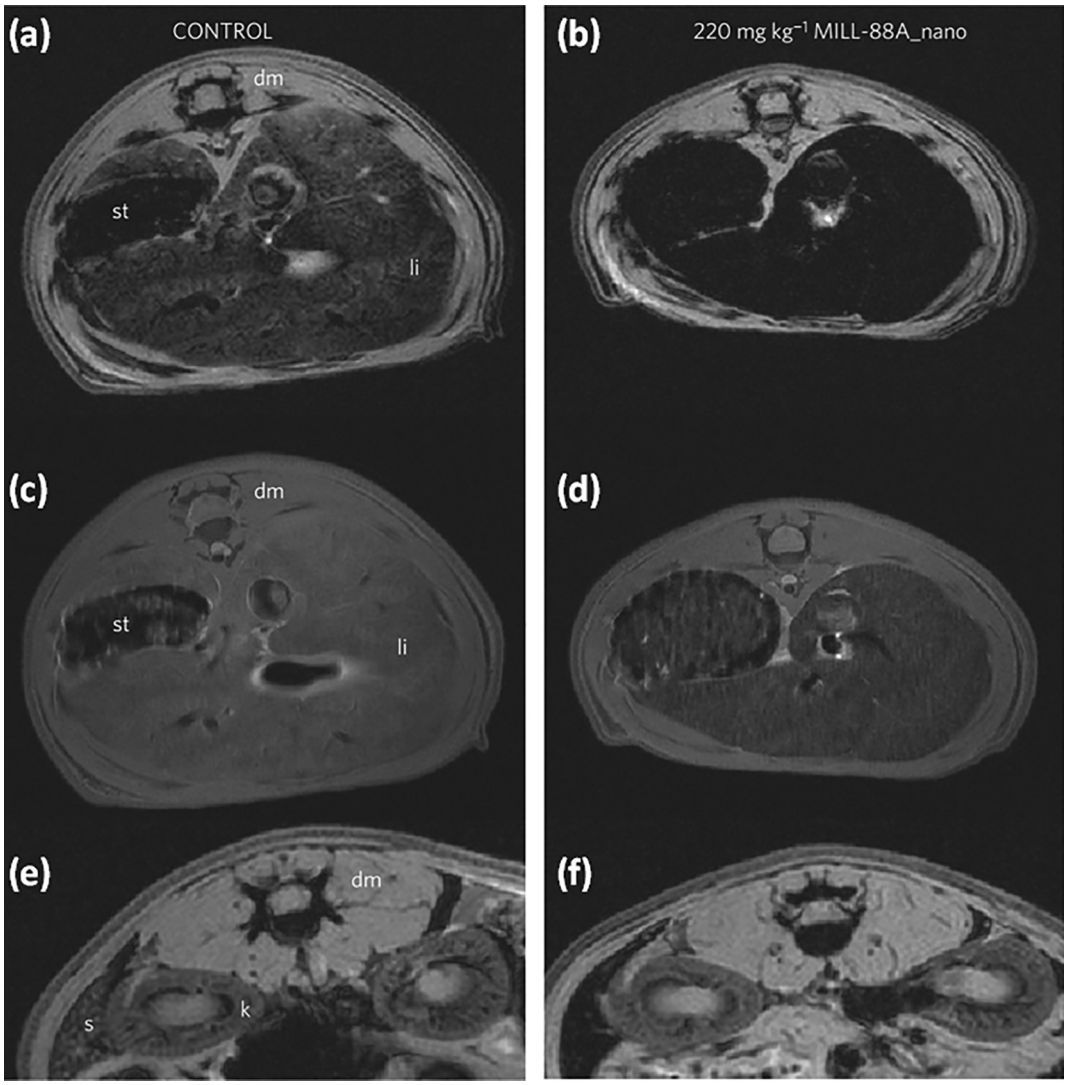

Fig. 10. T_2-weighted MR images of Wistar mice injected without MIL-88A (a, c, e) or with 220 mg/kg (e, d, f). The images were obtained by gradient echo (a, b, e, f) or spin echo (c, d) sequences. The images display the liver (a-d) or spleen (e, f) position after injection by 30 min. (dm, dorsal muscle; k. kidney; li, liver; s, spleen; st, stomach.) Reproduced from ref. 116 with permission of Nature Publishing Group, copyright 2010.

drugs. In 2010, Horcajada and collaborators reported the use of a series of non-toxic porous iron(III)-based nanoMOFs [116], i.e. MIL-53, MIL-88A, MIL-88Bt, MIL-89, MIL-100 and MIL-101-NH_2, as carriers of antineoplastic and retroviral drugs, including busulfan, azidothymidine triphosphate, doxorubicin or cidofovir, ibuprofen, caffeine, urea, benzophenone 3 and benzophenone 4. Despite the MOF stability concern, the stability was reported to be significantly improved by coating polymer materials. For example, coating polydimethysiloxane (PDMS) on the surface of MOF materials can greatly enhance their moisture or water resistance [143]; the platinum drug-loaded nanoscale coordination polymers (NCPs) are stabilized with silica shells to prevent rapid disintegration and effectively control the release of the platinum drugs [144]. Thanks to the protection of PEG in this work [116], these PEG-modified nanoMOFs possess good physiological stability and achieve controlled drug release without "burst effect". The sustained release of doxorubicin from nanoMIL-100 lasts up to 13 days, and the release amount is up to 100%, which is unmatched by other previous drug carriers (Fig. 11). This work has proved the great superiority of nanoMOFs as drug carriers and played a guiding role in the following progress.

Whereafter, Horcajada and co-workers investigated the in vivo metabolism and excretion of three porous Fe^{3+}-based nanoMOFs, including Fe-MIL-100, Fe-MIL-88A and 88B_4CH_3 [145]. After intravenously injecting high doses of these nanoMOF particles (up to 220 mg kg^{-1}) into female Wistar rats, the biodistribution and elimination of the nanoparticles were measured. The results showed that after a period of time, these nanoMOFs could be degraded into their constituents, such as iron and organic ligands, and then excreted from the body in the form of urine and feces, which confirms the excellent biosecurity of the biodegradable iron(III) carboxylate nanoMOFs for biomedical applications.

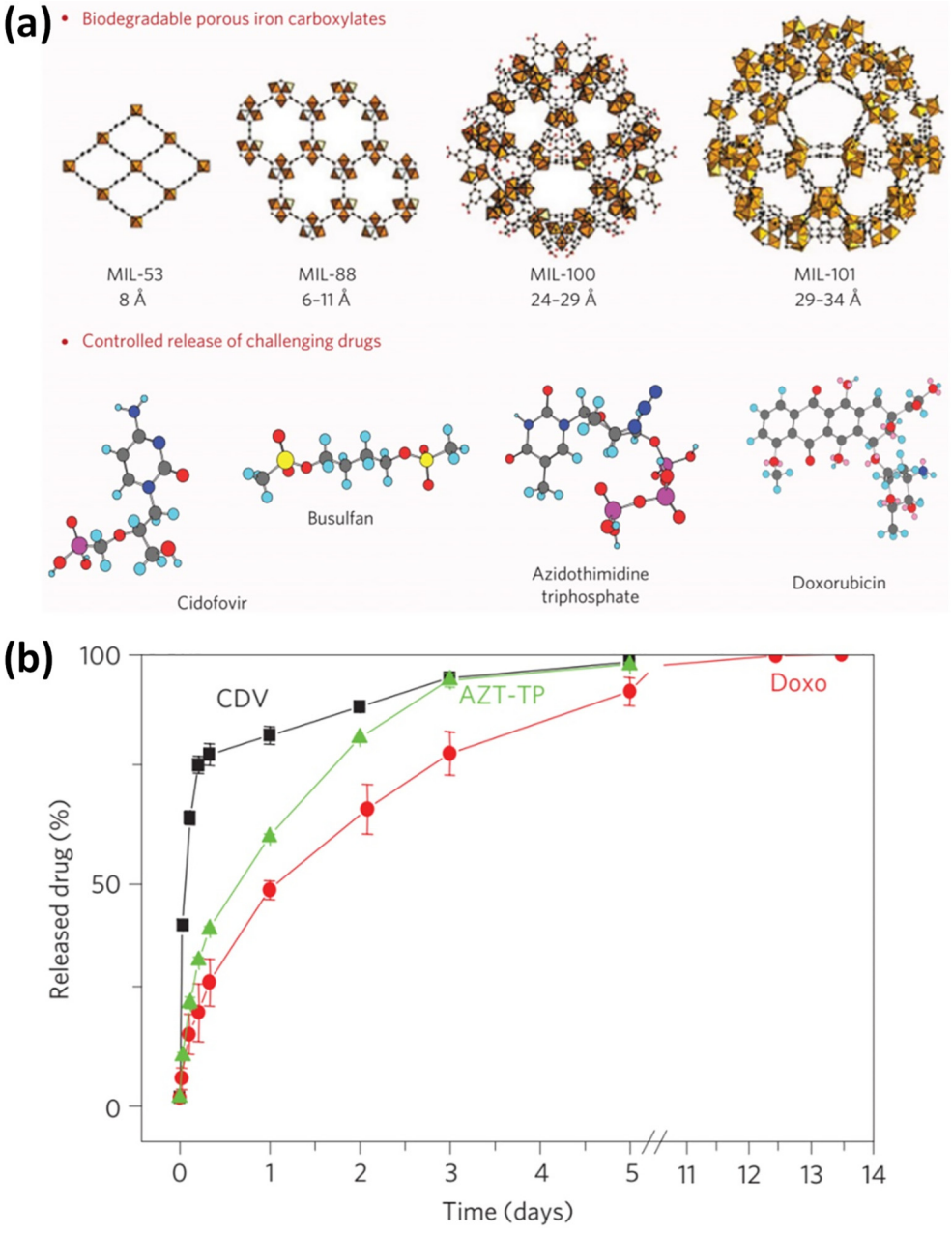

Fig. 11. (a) Schematic showing four porous iron-based nanoMOFs for drug delivery. (b) The released curves of cidofovir (black), doxorubicin (red) and azidothymidine triphosphate (green) under 37 °C in PBS solution from nanoMIL-100. Reproduced from ref. 116 with permission of Nature Publishing Group, copyright 2010.

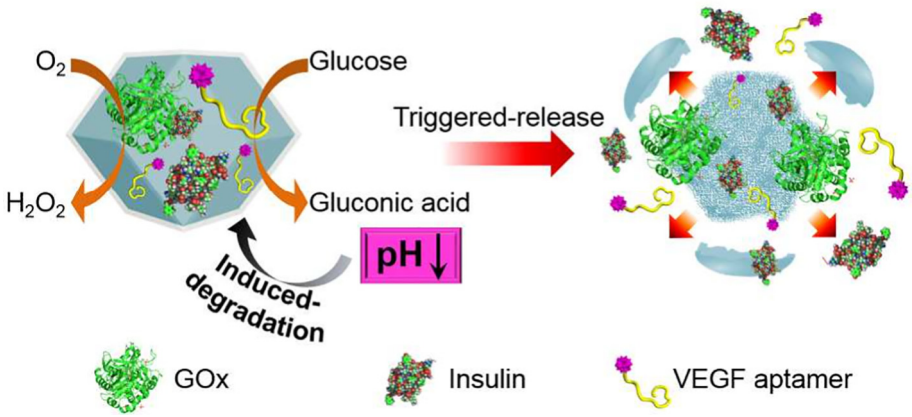

Fig. 12. Schematic synthesis of the insulin or VEGF aptamer/GOx-loaded ZIF-8 nanoMOF and the pH-induced degradation through the GOx-catalysed oxidation of glucose to gluconic acid. Reproduced from ref. 162 with permission of American Chemical Society, copyright 2018.

Another advantage of MOF as a drug carrier is that it can carry a wide variety of drugs. Deng and coworkers prepared four isoreticular Ni-MOF-74 analogues, i.e. Ni-IRMOF-74-II, -III, -IV, and -V, with adjusted pore size from 2.2 to 4.2 nm to effectively coat single-stranded DNA (ssDNA), and achieved invertible interaction between ssDNA and the as-prepared nanoMOFs. By modifying the synthetic conditions, nanosized Ni-IRMOF-74-II and -III crystals can be obtained with particle size around 100 nm. Furthermore, these two nanoMOFs were used for the transportation of ssDNA into cells which cannot be effectually transfected with conventional transfection agents. In addition, Ni-IRMOF-74-II and -III with the weaker forces of attraction between the nanoMOFs and ssDNA could transport ssDNA into cells and release them, showing great potential in intracellular transmission [146]. Apart from that, ZIF-8 is an outstanding representative for drug delivery, which is constructed by zinc ions and 2-methylimidazole and possesses unique merits such as high porosity and stability, good biosecurity, pH-induced degradability. Nano-sized ZIF-8 [147–150] is relatively convenient to prepare and has been widely used as nanocarriers for the loading of various agents including some functional inorganic nanoparticles, the small molecule anticancer drugs and some large molecule cargos such as enzymes, peptides, proteins [118,151–161]. Recently, Willner and co-workers encapsulated two drugs (e.g. insulin and anti-vascular endothelial growth factor aptamer (VEGF aptamer)) and glucose oxidase (GOx) into ZIF-8 nanoparticles to build a glucose-responsive vehicle for drugcontrolled release [162]. The nanohybrids-induced acid microenvironment results in the degradation of ZIF-8 nanoparticles and the release of the loaded drugs (Fig. 12). Finally, the synergistic effect of double-drugs will greatly improve the therapeutic efficiency.

Furthermore, Willner and co-workers continued to use ZIF-8 as the carrier to simultaneously load β-galactosidase, glucose oxidase, and horseradish peroxidase. β-galactosidase can first convert lactose to glucose. Whereafter, glucose oxidase can convert glucose to gluconic acid and hydrogen peroxide (H_2O_2) in the presence of oxygen. Then, horseradish peroxidase can convert amplex red to resorufin with the assistance of H_2O_2. Finally, the multienzyme-integrated MOF system can significantly enhance the catalytic cascades activity [163].

3.3. NanoMOFs as therapeutic agent for cancer

In addition to being used as carriers of anticancer drugs for tumour treatment, some functional MOF materials can not only act as carriers, but also can be directly used as therapeutic agent for cancer. Porphyrinic-based MOFs are one of the best representatives. In 2014, Lin and coworkers reported a kind of porphyrin-based nanoMOF for photodynamic therapy (PDT) of cancer [120]. The DBP-UiO nanoplate with 100 nm diameter and 10 nm thickness was obtained by reacting 5,15-di(pbenzoato)porphyrin (DBP) and Hf^{4+} through a solvothermal method. The porphyrin loading of the nanoplate was as high as 77 wt% and the results showed that the production of singlet oxygen ($^1O_2$) increased by at least two times compared with that of free porphyrin. Finally, the DBP-UiO nanoMOF showed enhanced PDT efficiency for head and neck tumour cells.

Zhou and coworkers reported a series of porphyrinic MOFs with different topologies, i.e. PCN-222, PCN-223, PCN-224 and PCN-225, which were constructed by Zr_6 clusters and TCPP or TCPP(M) (M = Ni, Cu, Zn, Co, Mn or Fe) [164–166]. In 2016, Zhou and collaborators further developed a size-controlled synthesis of PCN-224 for PDT (Fig. 13). In this study, a wide size range of PCN-224 nanoparticles from 30 to 190 nm were prepared by introducing benzoic acid as a modulator. After being modified with folic acid, these nanoparticles were examined for size-dependent cellular uptake and in vitro PDT, and the result showed that the 90-nm PCN-224 nanoparticles had the best PDT effect, suggesting a promising PDT therapeutic agent [119].

Dong and coworkers reported a novel UiO-66 type of nanoMOF-based photosensitizer (UiO-66-TPP-SH), which was produced by combining the nanosized UiO-66 with S-ethylthiol ester monosubstituted metal free porphyrin (TPP-SH) via a post-synthetic method. The surface-modified nanoMOF (about 150 nm in diameter) with porphyrin PS can maintain the size, crystallinity and structural characteristics of the original MOF. In addition, in vitro experiments showed that the UiO-66-TPP-SH exhibited more effective PDT effect on cancer cells [167].

Radiotherapy (RT) has been widely used clinically due to its high efficiency to kill cancer cells. However, high-dose radiation can cause damage to normal cells while acting as a cure. High-Z metals such as Au, Hf, and Ru are usually used for radiosensitizers for enhanced radiotherapy. For instance, Au nanoparticles or clusters can enhance the radiotherapy [168–172]. Hf-based MOF has been developed as an efficient agent for radiotherapy [122,173]. Recently, Lin and co-workers reported Hf-DBB-Ru [DBB-Ru = bis(2,2′-bipyridine)(5,5′-di(4-benzoato)-2,2′-bipyridine) ruthenium (II) chloride] as a mitochondria-targeted nanoMOF for RT-RDT. Due to the higher atomic number, both Hf and Ru can act as radiosensitizers to enhance the efficiency of RT. Under X-ray irradiation, hydroxyl radical (·OH) and $^1O_2$ generated concurrently from

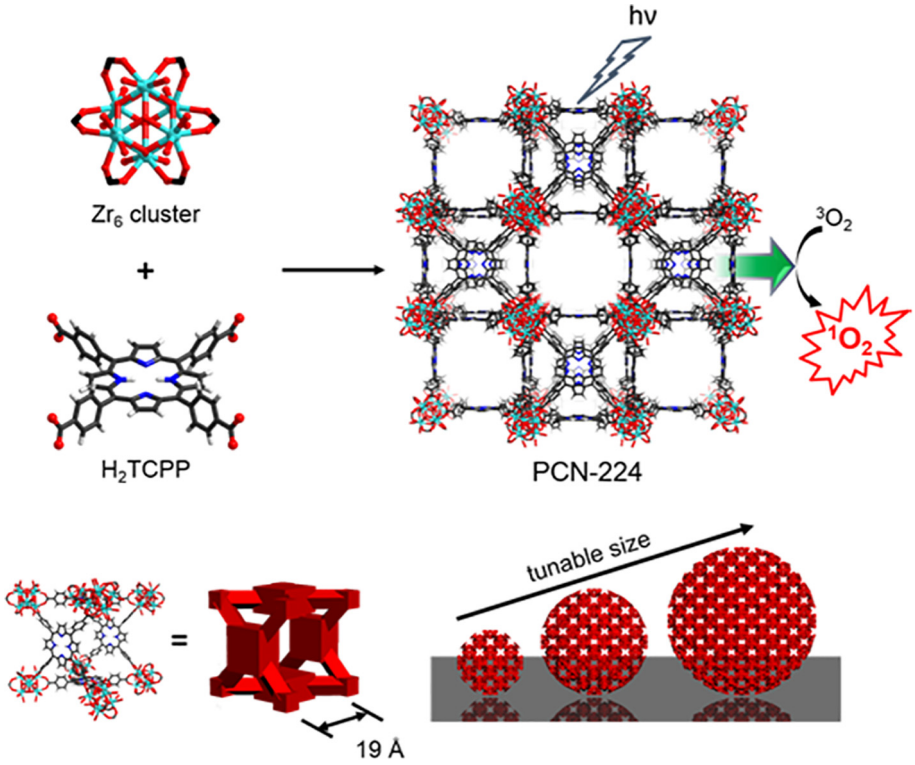

Fig. 13. Schematic illustration of PCN-224 structure and the spherical PCN-224 nanoparticles on the basis of cubic units with different sizes. Reproduced from ref. 119 with permission of American Chemical Society, copyright 2016.

the nanosized Hf-DBB-Ru. Both in vitro and in vivo experiments showed that the mitochondria-targeted RT-RDT could significantly kill the tumour cells [174].

Recently, a hierarchical W_{18}@Hf_{12}-DBB-Ir structure, which simultaneously contains three high-Z components, i.e. Hf, Ir and W, was reported. Under the irradiation of X-ray, W_{18}@Hf_{12}-DBB-Ir can generate ·OH from Hf_{12} SBUs, $^1O_2$ from DBB-Ir ligands, and superoxide generation from W_{18} polyoxometalates, respectively. The nanoMOF showed excellent anticancer efficacy via the synergistic killing effect of different reactive oxygen species (ROS) [175].

In general, porphyrin-based MOFs not only exhibit excellent PDT effect, but also can load drugs or functional components to achieve enhanced cancer therapy [168]. Yin and coworkers used a nanoscale porphyrinic MOF, PCN-222, to load doxorubicin (DOX) for synergistic chemotherapy and PDT [176]. Due to the non-covalent interaction between PCN-222 and DOX, the PCN-222 nanoparticles possessed a 109% DOX load and pH-response release. Further tests showed that drug release was slow under normal physiological conditions, but it was accelerated under slightly acidic conditions. This drug release behavior can enhance the treatment efficacy on tumour cells and lower the side effects on normal cells. In addition, 59.8% of porphyrins in PCN-222 produced excellent PDT efficacy. Under the irradiation of 655-nm laser, the apoptosis of 90% tumour cells was achieved by the synergistic treatment of DOX@PCN-222. Compared with PDT or chemotherapy alone, DOX@PCN-222 exhibited a higher therapeutic effect on HepG2 tumour-bearing mice, indicating that this porphyrin-based MOF platform is highly effective for synergistic PDT and chemotherapy.

Internal hypoxia is ubiquitous in solid tumours. To solve this problem, Qu and co-workers prepared a platinum-loaded PCN-224 (PCN-224-Pt) nanoMOF platform for enhanced PDT [177] (Fig. 14). Due to the high level of H_2O_2 in the tumour microenvironment, the Pt nanoparticles can catalyze H_2O_2 to produce O_2 within tumour, thereby promoting the production of cytotoxic $^1O_2$ and killing tumour cells. In vitro experiments showed that the cell apoptosis with PCN-224-Pt under red laser irradiation was significantly higher than that of PCN-224 under low oxygen conditions. In the H22 tumour-bearing mouse model, the anti-tumour performance in vivo confirmed that the injection of PCN-224-Pt after irradiation completely inhibited tumour growth, while the injection of PCN-224 after PDT only partially inhibited tumour growth.

To address oxygen depletion in the tumour, more and more attention has been paid to type I PDT, which is independent on oxygen level. Recently, a novel Ti-TBP nanoMOF which consists of Ti-oxo SBUs and 5,10,15,20-tetra(p-benzoato)porphyrin (TBP) ligands was used for type I PDT. First, Ti-TBP can produce $^1O_2$ under the irradiation of light. In addition, electron transfer between the metal center and the ligand promoted the generation of superoxide, H_2O_2, and ·OH. By gathering four different ROS, Ti-TBP-mediated PDT showed high anti-cancer efficiency [178].

Cai et al. reported a biodegradable nanoMOF therapeutic agent for enhanced PDT by simultaneously supplying oxygen and reducing the amounts of intracellular glutathione (Fig. 15). The nano CuTz-1 with size of about 100 nm was first prepared. In vitro experiment showed that this cupric ion-based MOF could generate ·OH and O_2 in the presence of H_2O_2 by a Fenton-like reaction under light irradiation. And the nanoparticles can maintain their original structure and properties before and after light exposure. Moreover, due to the mutual attraction of copper ions and oxygen, the CuTz-1 nanoparticles could carry oxygen into tumour cells, which could relieve intracellular hypoxia. Additionally, CuTz-1 could consume intracellular glutathione, thus enhancing the efficiency of PDT again. After being modified by a biocompatible polymer F127 and via tail intravenous injection, the nanoparticles showed high anti-tumour efficiency through a synergistic effect. Moreover, after

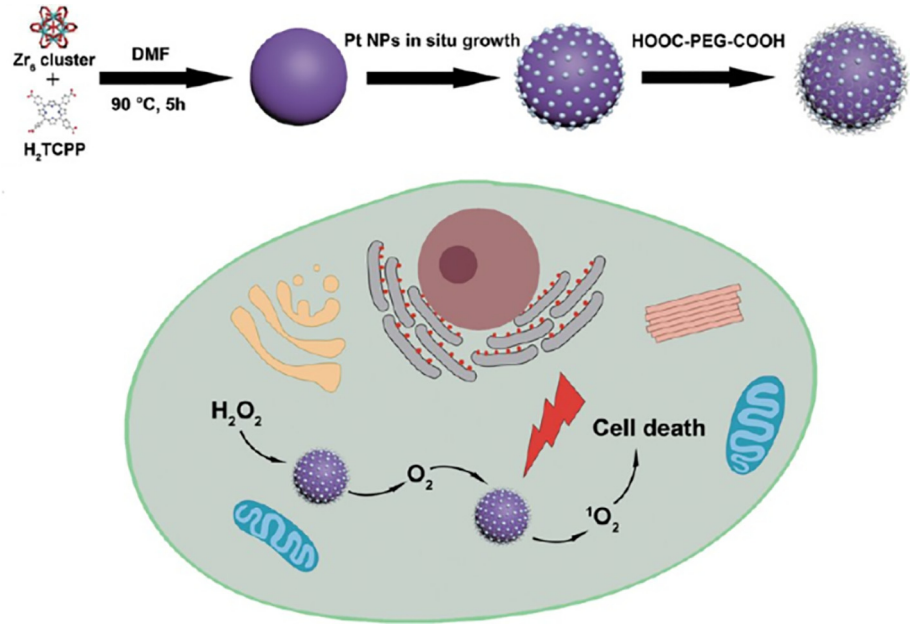

Fig. 14. Synthetic route of PCN-224-Pt and schematic diagram of PCN-224-Pt used to enhance PDT. Reproduced from ref. 177 with permission from the American Chemical Society, copyright 2018.

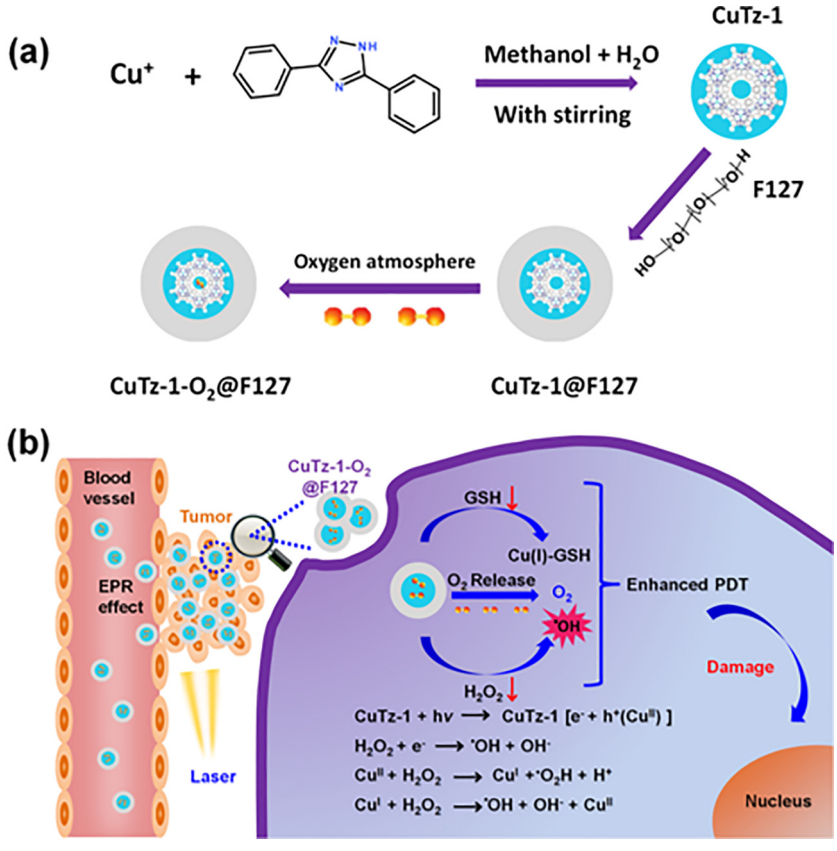

Fig. 15. (a) Schematic of preparing CuTz-1-O_2@F127 nanoparticles and (b) for enhanced PDT. Reproduced from ref. 179 with permission from Wiley-VCH, copyright 2019.

being injected into mice via tail vein, the CuTz-1-O_2@F127 was biodegradable and could be excreted in the form of feces and urine, indicating significant prospects in the clinical application [179].

In addition to PDT, a few nanoMOF platforms have been reported to be used for photothermal therapy (PTT) of tumours. Xie and coworkers coated NIR-absorbing polymer (polyaniline, PAN) on the surface of nanoUiO-66 to build UiO-66@PAN (ca. 100 nm). Under the irradiation of 808-nm laser, the photothermal conversion efficiency of UiO-66@PAN reached 21.6% and it showed efficient PTT both in vitro and in vivo [180]. In another work, the

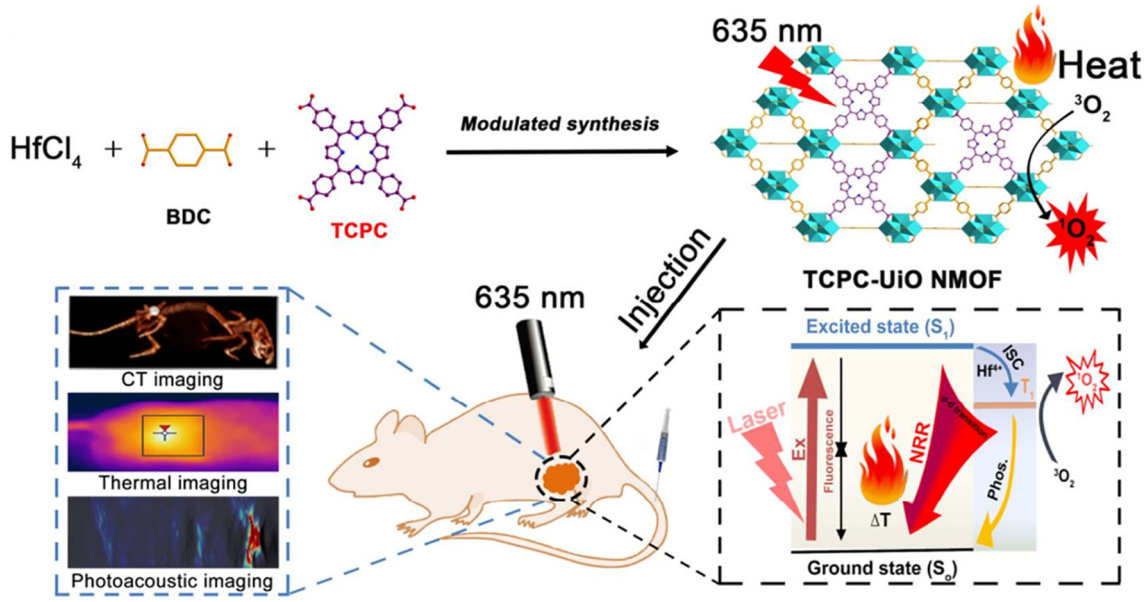

Fig. 16. Synthetic procedure of TCPC-UiO nanoMOF and schematic illustration of heat and $^1O_2$ generation under laser irradiation and combination therapy in vivo guided by CT/thermal/photoacoustic imaging. Reproduced from ref. 181 with permission from the American Chemical Society, copyright 2018.

same group prepared TCPC-UiO by adding photosensitive chlorin into Hf-UiO-66 without changing its original topological structure by using a simple mixing component strategy. The TCPC-UiO with an average size of 100–130 nm has high photostability, good biocompatibility and effective photodynamic and photothermal therapeutic effects attributed to the spatial arrangement of TCPC ligands. Moreover, while the Hf element enables the nanoscale TCPC-UiO platform to have the CT imaging function, it also greatly enhances the phototherapy under laser irradiation due to the heavy atomic effect. Good photothermal conversion efficiency is conducive to the follow-up use of TCPC-UiO in photoacoustic imaging and PTT (Fig. 16). In vivo tests showed that the as-prepared TCPC-UiO had distinct anti-tumour effect on tumour-bearing mice, and its tumour inhibition rate was up to 90% [181].

4. NanoMOFs for enhanced catalysis

In the catalytic reaction, the phenomenon of accelerating the chemical reaction rate due to the intervention of the catalyst is called catalysis. The catalyst interacts with the reactants, changing the reaction pathway, thereby reducing the activation energy of the reaction, which is the reason why the catalyst can increase the reaction rate.

It is of interest to employ active sites on the metal nodes and/or organic linkers of MOFs, as it enables the on-site separation of controlled components for catalysis [182,183]. In addition, although the profitable porosity of MOFs is beneficial for catalysis, the approachability of active sites and mass transfer still remain challenging, especially when the catalytic reaction involves large substrates, which are subject to diffusion to internal catalytic sites. One method to improve the spread of reactants and products in MOF materials is to manufacture nanoMOFs to reduce diffusion barriers. In the earlier time, Kitagawa and coworkers synthesized different-sized Yb-MOF-76 and investigated the catalytic activity on isomerization reaction of 1-hexene. The result revealed that the catalytic performance of submicrosized Yb-MOF-76 was higher than that of microsized Yb-MOF-76. Due to the rapid diffusion of the substrate to the internal pore surface, it can lead to a large amount of actual functional catalytic sites [184].

Farha and coworkers reported a Zr-based mesoporous MOF (i.e., NU-1000) and investigated the effect of crystallite size on the hydrolysis of methyl paraoxon. Different sizes of NU-1000 particles from nanoscale to microscale were synthesized (Fig. 17a-d). Under certain conditions, the catalytic activity clearly increases with the decreased size of NU-1000 (Fig. 17e), because smaller particles show a larger external surface area that allows reactants to permeate more rapidly into NU-1000 nanoparticles [185]. In another related example, Farha and coworkers prepared a Zr-based MOF, NU-1003, which has large mesopores (approximately 4.5 nm) and allows the loading of the nerve agent hydrolyzing enzyme, organophosphorus acid anhydrolase. Meanwhile, nanosized NU-1003 was prepared to accelerate diffusion of the nerve agent to go through the MOF-enzyme hybrids. As a result, the activity of the hybrid was better than that of the free enzymes [186]. Significantly, it is a difficult task to maintain or exceed the activity of free enzymes compared with composites. This work demonstrated the powerful advantages of nanoMOF materials as catalytic carriers.

Another key point in the catalytic application of nanoMOF materials is their monodispersity. In fact, although many nanoMOFs can be synthesized into monodispersed particle sizes, many more are crystallized in a multi-dispersed manner. Considering that the size of nanoMOF has an important effect on the catalytic activity, it is important to ensure that the sample contains monodispersed particle sizes before concluding on the catalytic activity. Wang and co-workers reported a nanoscaled copper-based MOF as a heterogeneous catalyst for aerobic epoxidation of olefins and oxidation of benzylic and allylic alcohols. When copper-based MOFs with different sizes were used, the nanosized Cu-MOF-2 showed best catalytic reactivity. This catalytic activity of nano Cu-MOF-2 was further extended to the oxidation of alcohol with similar reaction conditions. This result demonstrated that the increased monodispersity can effectively enhance catalytic performance [187].

In another typical example, Schmidt and coworkers recently presented a general method to synthesize a nanoMOF/polymer hybrid with stimuli-responsive dispersibility and enhanced photocatalytic performance in liquid phase [188]. To be specific, by employing hollow pollen as initial substrate, an environment-responsive polymer, poly(2-(dimethylamino)ethyl methacrylate)

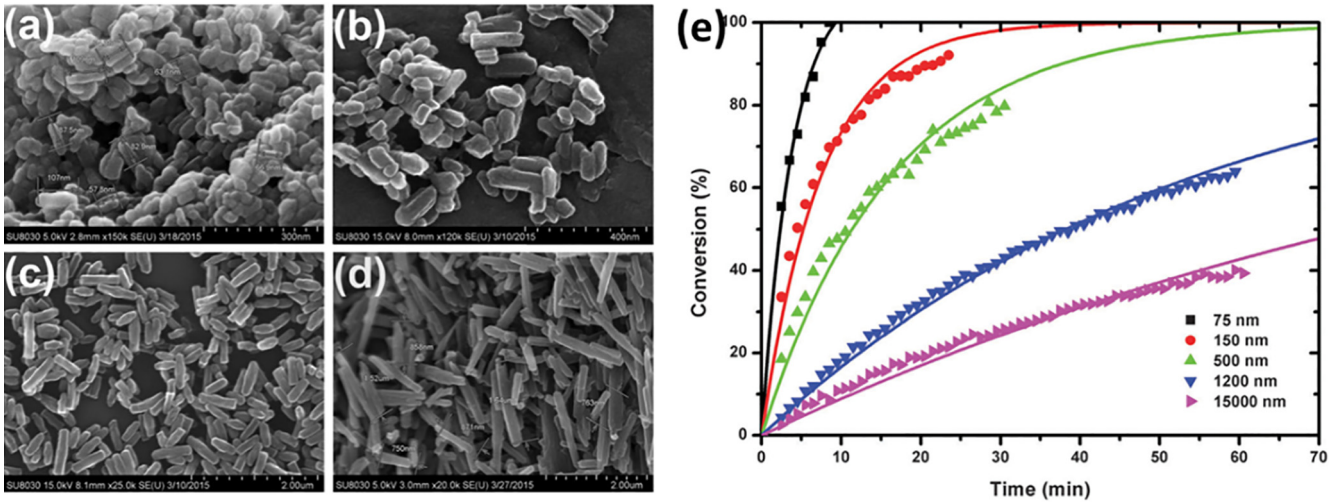

Fig. 17. SEM images of NU-1000 nanoparticles with different sizes. (a) 50–100 nm; (b) 100–200 nm; (c) 300–700 nm; (d) 800–1600 nm. (e) Hydrolysis rates of methyl paraoxon by using NU-1000 nanoparticles with average sizes ranging from 75 nm (black), 150 nm (red), 500 nm (green), 1200 nm (blue), to 15000 nm (pink). Adapted from ref. 185 with permission from Royal Society of Chemistry, copyright 2015.

(PDMAEMA) was then coated on the surface, finally the nanosized $Cu_2(bdc)_2(dabco)$ can be incorporated into the pollen-PDMAEMA composites (P-pollen) to concurrently increase dispersibility and enhance the photocatalytic performance. Furthermore, the catalytic performance can be controlled by a stimulable transition of the PDMAEMA chains exposing or hiding the catalytic sites of $Cu_2(bdc)_2(dabco)$, respectively (Fig. 18).

Very recently, Fischer and coworkers reported on the preparation of surface-anchored nanoUiO-66 with PDMS for enhanced catalysis (Fig. 19). The surface-coated PDMS can prevent nanoMOFs from agglomerating and maintain high specific surface area. Therefore, the structure, particle size and surface functional groups of the nanoMOFs did not change before and after the catalytic reaction. However, the colloidal nanoMOFs agglomerated after the reaction. As a result, the PDMS-modified nanoUiO-66 exhibited a boost in activity compared with the block-shaped UiO-66 and colloidal-dispersed nanoUiO-66 in the cyanosilylation of benzaldehyde. In addition, the performance of the surface-anchored nanoMOFs was much better than that of block-shaped MOFs and defect-engineered MOFs in other catalytic systems including the cycloaddition reactions of carbon dioxide and propylene oxide to propane carbonate. This work greatly highlighted that nanoMOFs with high monodispersity had resplendent application prospects in the field of catalysis [189].

In addition, the nanoMOFs have been investigated as the hosts for guest active species toward catalysis. Jiang and coworkers fabricated a Pd nanocubes@ZIF-8 core-shell complex by encapsulating the Pd nanocubes in nanosized ZIF-8 (250–350 nm). This nanocomposite can selectively and effectively catalyze the hydrogenation of olefins under the conditions of room temperature, 1 atm H_2 and light irradiation. The Pd cores can produce plasmonic photothermal effects. The ZIF-8 shell performs a triple function: it can be used as a "molecular sieve" to filter olefins with certain sizes, stabilize Pd nanocubes and accelerate the reaction by enriching H_2. It is worth noting that the catalytic efficacy with 60 mW cm^{-2} full-spectrum or 100 mW cm^{-2} visible-light

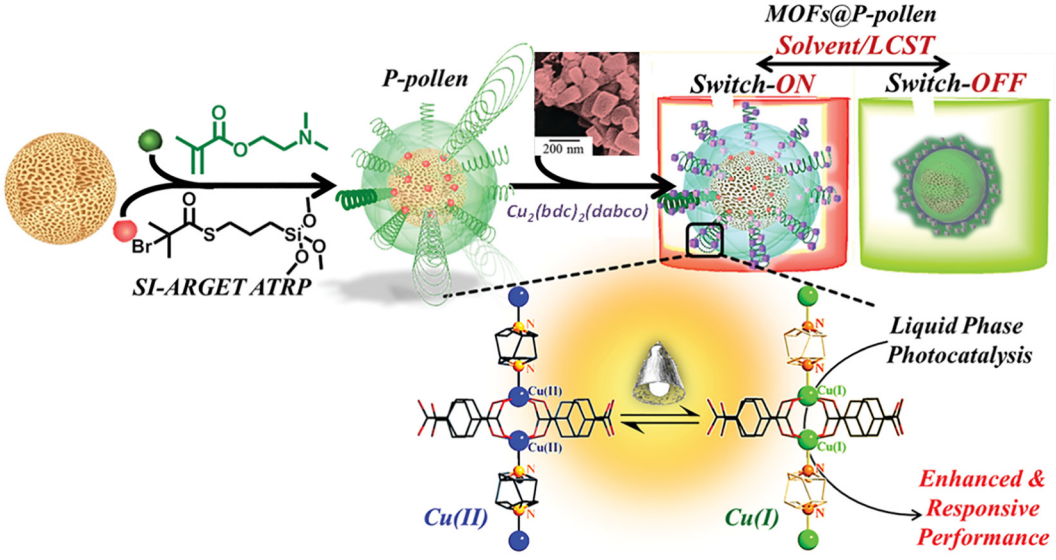

Fig. 18. (a) Schematic illustration of the nanosized $Cu_2(bdc)_2(dabco)$@P-pollen composite for enhanced liquid-phase photocatalytic reactions. Adapted from ref. 188 with permission from Royal Society of Chemistry, copyright 2019.

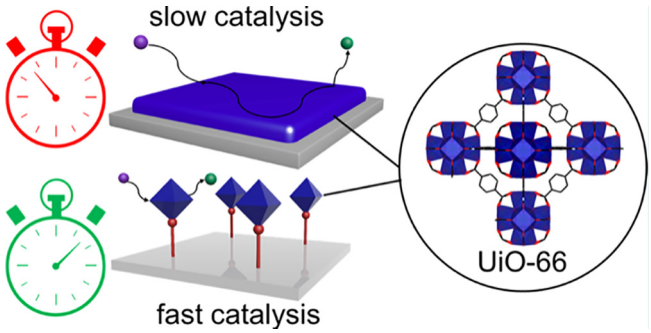

Fig. 19. Schematic comparison of catalytic rates of surface-anchored nanoMOFs with bulk MOFs or colloidal-dispersed MOFs. Reproduced from ref. 189 with permission from the American Chemical Society, copyright 2020.

irradiation at room temperature was similiar to that under conditions of heating at 50 °C. In addition, such a catalyst is stable and easy to recover during the reaction. This is the first combination of the plasma-driven photothermal conversion performance of metal nanoparticles with the excellent properties of nanoMOFs for efficient and selective catalysis [190].

The 1-D MOF nanomaterials have been reported toward efficient catalysis. As a representative study, PA-6@TiO_2@UiO-66-NH_2 and PA-6@TiO_2@UiO-67 MOF-nanofiber structures exhibited remarkable catalytic performance for the decomposition of chemical warfare agents (CWA), in which the two MOF nanofiber catalysts enabled short half-life of simulant 4-nitrophenyl phosphate (DMNP) and high conversion in 60 min. In addition to DMNP, the MOF-nanofiber composites can be also used for the degradation of nerve agent GD. The three MOF-nanofiber composites all showed high GD destruction speed and conversion rate within 10 min, indicating the good prospects of MOF-nanofiber for degradation of CWA [109].

5. NanoMOFs for energy

While nanoMOFs have achieved great success in the field of biomedicine, the energy-related applications have not been fully explored. Particularly, the larger external surface areas and smaller sizes make it easier for them to combine closely with other materials to form hybrid materials for use in energy, such as in solar cells, batteries and supercapacitors. Recently, nanoMOFs have been regarded as promising candidates for cathode materials with excellent performances. Ho and coworkers coated MOF-525 nanoparticles with size of about 200 nm and the conductive sulfonated polythiophene (s-PT) on carbon cloth to prepare a flexible counter electrode [191]. The zirconium oxo clusters and porphyrin ligands in MOF-525 acted as redox active sites for I^-/I^{3-} palingenesis, and the pores provided more channels for catalytic sites. The composite layer wrapped the 1-D fibers of the carbon cloth to form a core-shell structure, where the core provided the major electronics transport and the shell acted as a catalyst (Fig. 20a, b). Adjusting the content of MOF-525 nanoparticles can equilibrate the catalytic and conductive effects. The performance of 3 wt% MOF-525 was the highest, and the battery efficiency could reach up to 8.91%, and it can be further increased to 9.75% in dim light (Fig. 20c).

MOF nanocrystals can also be used in supercapacitors. Wang and coworkers prepared a flexible MOF-based supercapacitor by coating nanosized ZIF-67 with sizes of about 300 nm on a carbon cloth, followed by the coating of polyaniline. The open pores in MOF made the electrolyte easy to diffuse, while polyaniline enabled electrons to enter the MOF surface, thus obtaining a high surface capacitance [192]. In another related study, a polyoxymetalate-based nanoMOF with size smaller than 100 nm were coated on polypyrrole. Thanks to the excellent electron transfer capability of the polyoxymetalate, the conductive ability of the nanoMOF/polypyrrole as well as the accessibility of active sites in the nanoMOFs, the electrode and the symmetric supercapacitor showed a high performance [193].

NanoMOFs as the hosts for guest active species have also been applied to the energy field. Jiang and coworkers encapsulated Pt nanoparticles inside nanosized UiO-66-NH_2 to construct Pt@UiO-66-NH_2 nanocatalyst for photocatalytic hydrogen production by water splitting. Through ultrafast transient absorption and multiple techniques, they proved that the Pt@UiO-66-NH_2 could shorten the electron-transport distance, thus promoting the separation of electron-hole. Finally, Pt@UiO-66-NH_2 hybrids exhibited good charge-carrier utilization and thus achieving a high photocatalytic activity for hydrogen production. Moreover, the Pt@UiO-66-NH_2 nanocatalyst possessed excellent stability and recyclability thanks to the perfect confinement of Pt nanoparticles in the nanoMOF. This study provided a promising perspective for nanoMOF-based materials to be used in solar energy conversion [194].

1-D MOF nanomaterials also have good application prospects in energy. Wen et al. prepared nickle MOFs/carbon nanotubes (Ni-MOF/CNTs) hybrids, which had great electrochemical performance thanks to the synergetic effects of the unique structure of Ni-MOF and the highly conductive CNTs. To further investigate the capacitive property of the electrode, an asymmetric supercapacitor device by employing Ni-MOF/CNTs as positive electrode and reduced graphene oxides/graphitic carbon nitride (rGO/g-C_3N_4) as negative electrode was prepared and showed a high energy

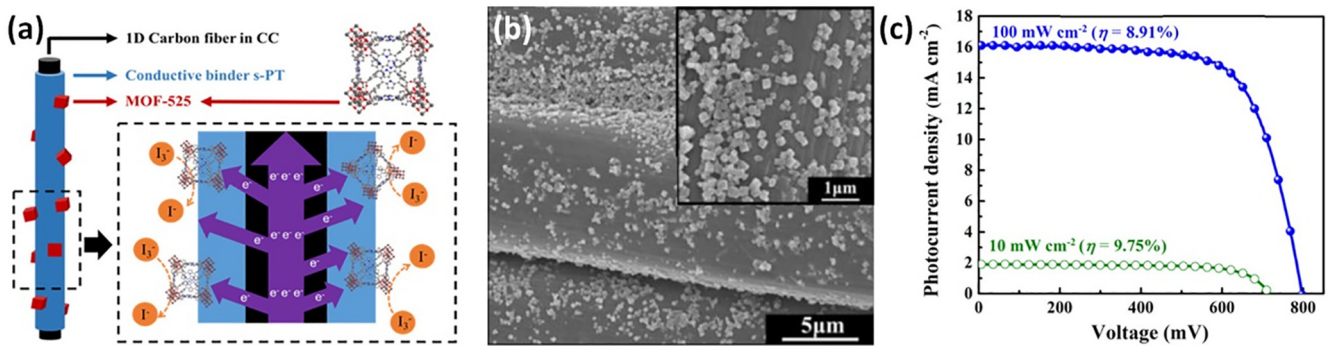

Fig. 20. (a) The core-shell structure of MOF-525/s-PT composite film coated on the carbon cloth. (b) SEM images of 3 wt% MOF-525/s-PT. Inset is the high magnification. (c) Photocurrent density-voltage curves of the DSSC with 3 wt% MOF-525/s-PT, illuminated under 10 and 100 mW cm^{-2}, respectively. Adapted from ref. 191 with permission from Elsevier Ltd, copyright 2017.

density of 36.6 Wh kg^{-1} at a power density of 480 W kg^{-1}. In addition, this supercapacitor showed a long cycle life after 5000 charge/discharge measurements [195].

Zhao and coworkers prepared a kind of multilevel carbon nanotubes/nickel-trimesic acid hybrids (MWCNTs@Ni(TA)) by a solvothermal method. The results indicated that carboxyl-modified MWCNTs played a key role in inducing the change of Ni (TA) from spherical shape to nanoscale flower shape. Electrochemical tests indicated that the flower-shaped MWCNTs@Ni(TA) hybrids had a higher specific capacity and a better rate capability than the spherical Ni(TA). In addition, the MWCNTs@Ni(TA) electrode also possessed great cycling stability [196].

6. NanoMOFs for membrane separation

Gas separation membrane is a new technology that has developed rapidly in recent years. Different membranes have different permeability and selectivity for different kinds of gas molecules, thus a certain gas can be selected and separated from the gas mixture. MOF materials have received great attention because of their good gas storage/separation performance. In some early studies, the free-standing MOFs membranes have been successfully prepared for gas separation. Peng and co-workers prepared a kind of HKUST-1 free-standing membrane by employing copper hydroxide thin films as templates [197]. The obtained HKUST-1 membranes possessed excellent gas separation performance beyond Knudsen selectivity. The separation factor of the HKUST-1 membrane for H_2/CH_4, H_2/N_2, H_2/O_2 and H_2/CO_2 was 2.5, 3.3, 3.4 and 4.2, respectively.

Wu et al. reported the preparation of free-standing ZIF-8 membrane by using electrospun nanofibrous mats as templates [198]. When the 1:1 mixture of N_2/CO_2 was used to test the gas separation performance of the ZIF-8 membrane, it showed better CO_2 separation effect due to the high specific surface area and the stronger adhesive force of ZIF-8 to CO_2. The final separation factor of N_2/CO_2 was 2.4, showing good gas separation performance.

Although free-standing MOF membranes exhibit good gas separation performance, some disadvantages such as the fragility and lower permeability limit their further applications. Recent studies have shown that the membrane prepared by doping porous MOF materials into polymers or other matrices has excellent gas separation properties. Such composite materials can simultaneously integrate the processability of polymer (or other matrices) and the good separation performance of MOFs. Among them, nanoMOF-based hybrid matrix membranes composed of nanoMOFs bonded to polymer or other matrices show more excellent performance. First of all, in the present industrial applications, the thickness of a polymer membrane is usually about 100 nm. Therefore, it is more practical to use nanoMOFs to build a membrane. Secondly, smaller-sized MOF particles are easier to uniformly and closely integrate with matrices, thus improving the stability of the membrane. Thirdly, the composite membranes can simultaneously maintain the high selectivity of the nanoMOFs and the high permeability of the polymer. In this part, we will just review the recently representative progress of nanoMOFs for mixed matrix membranes, more comprehensive summaries can be referred to other reviews [199,200].

The polymer polyimide (PI) has been widely studied for gas separation because of its excellent permeability [201]. Jin and coworkers integrated nanoscale ZIF-8 with PI to prepare MOF/PI mixed matrix membranes for enhanced gas separation performance [202]. The surface of ZIF-8 nanoparticles (30–60 nm) was first coated a thin layer of polydopamine, which not only could protect the pores of ZIF-8 from choking, but also would enhance the affinity between ZIF-8 and the polymer PI. Whereafter, the PI polymer readily attached to the surface of polydopamine to construct nanoZIF-8/PI membranes, which combined the high selectivity of ZIF-8 with the high permeability of PI. The results showed that the gas separation performance of the membrane composites exceeded the most advanced Robeson upper bound for gas pairs of H_2/N_2, H_2/CH_4 and was close to the upper bound of O_2/N_2 gas pair.

In another work, Long and collaborators incorporated a series of nanoscale M-MOF-74 (M = Mg, Mn, Co, Ni) into the PI matrix to prepare MOF/PI membranes for the separation of ethylene and ethane [32]. The particle sizes of Co-MOF-74 and Ni-MOF-74 were 17 ± 3 and 18 ± 5 nm, respectively. While the sizes of Mn-MOF-74 and Mg-MOF-74 nanoparticles were relatively large, which were 100 ± 20 and 200 ± 50 nm, respectively. The as-prepared MOF/PI membranes possessed improved adsorption selectivity and increased permeability towards ethylene. In particular, thanks to their smaller sizes as well as the strong interactions between nanoMOFs and the polymer, the nanosized Co-MOF-74 and Ni-MOF-74 doped membranes could greatly enhance ethylene/ethane separation performance.

Many other polymers or matrices are also widely used to combine with nanoMOFs to produce composite membranes. Recently, Chen and coworkers reported several nanoMOF/organosilica composites on a tubular ceramic substrate for high gas separation performance [203]. Nanosized ZIF-8, MIL-53-NH_2 and CAU-1-NH_2 were first doped into organosilica to prepare MOF/organosilica hybrids. Due to high affinity between organosilica and ceramic substrate, the MOF/organosilica was then easily coated onto a tubular ceramic substrate (Fig. 21a). It is worth pointing out that the thickness of the as-prepared MOF/organosilicone layer is about 100 nm, and the very thin film plays a positive role in the subsequent separation application. Especially, the as-obtained ZIF-8 and MIL-53-NH_2 organosilicone nanocomposite membrane was proved to be one of the best MOF substrates. As shown in Fig. 21b, the ZIF-8/organosilica membrane has a high selectivity for H_2/N_2 and H_2/CH_4 mixtures. In particular, the selectivity of ZIF-8/organosilica towards the separation of H_2/CH_4 mixture was 26.5. The MIL-53-NH_2/organosilica membrane also exhibited great separation performance towards CO_2/CH_4 mixtures and the selectivity was 18.2. These two parameters are much higher than those of reported pure MOF membranes.

In another work, Sivaniah and coworkers synthesized a mixed matrix membrane to effectively capture CO_2 via dispersing amine-modified nanosized UiO-66 with particle size of 20–30 nm into PIM-1 polymers [204]. The nanoMOF in the hybrid can enhance its dispersion in the polymer matrix and minimizes the formation of non-selective micropores around the particles. Amine-modified UiO-66 can increase the mutual effect with the PIM-1 matrix. Finally, the high-performance membrane was obtained and showed high permeability selectivity for CO_2/N_2 separation.

Helms and coworkers reported the interposition of a kind of 1-D mmen-Mg_2(dobpdc) nanorods with a size of 100–200 nm into the polymer to prepare the MOF/polymer membrane for CO_2/N_2 separation (Fig. 22). First of all, the mmen-Mg_2(dobpdc) has shown good adsorption performance towards CO_2. The nanoMOF/polymer can be used to increase the solubility of CO_2 gas in the membrane, thereby increasing its permeability. In addition, the use of nanosized mmen-Mg_2(dobpdc) also promoted the CO_2/N_2 separation efficiency. Finally, when the nanoMOF/polymer membrane was used in the CO_2/N_2 separation experiments, the permeability of CO_2 was doubled, and the selectivity of CO_2/N_2 separation was also improved accordingly [205].

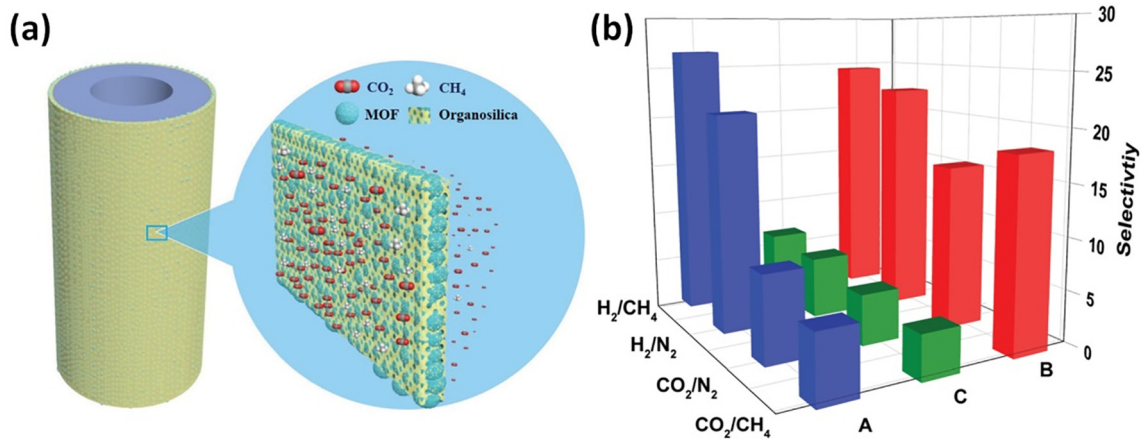

Fig. 21. (a) Schematic of the nanoMOF/organosilica complex membrane on an alumina substrate for gas separation. (b) The selective separation of H_2/CH_4, H_2/N_2, CO_2/CH_4 and CO_2/N_2 by the ZIF-8/organosilica (A), MIL-53-NH_2/organosilica (B) and CAU-1-NH_2/organosilica (C) membranes. Adapted from ref. 203 with permission from Royal Society of Chemistry, copyright 2017.

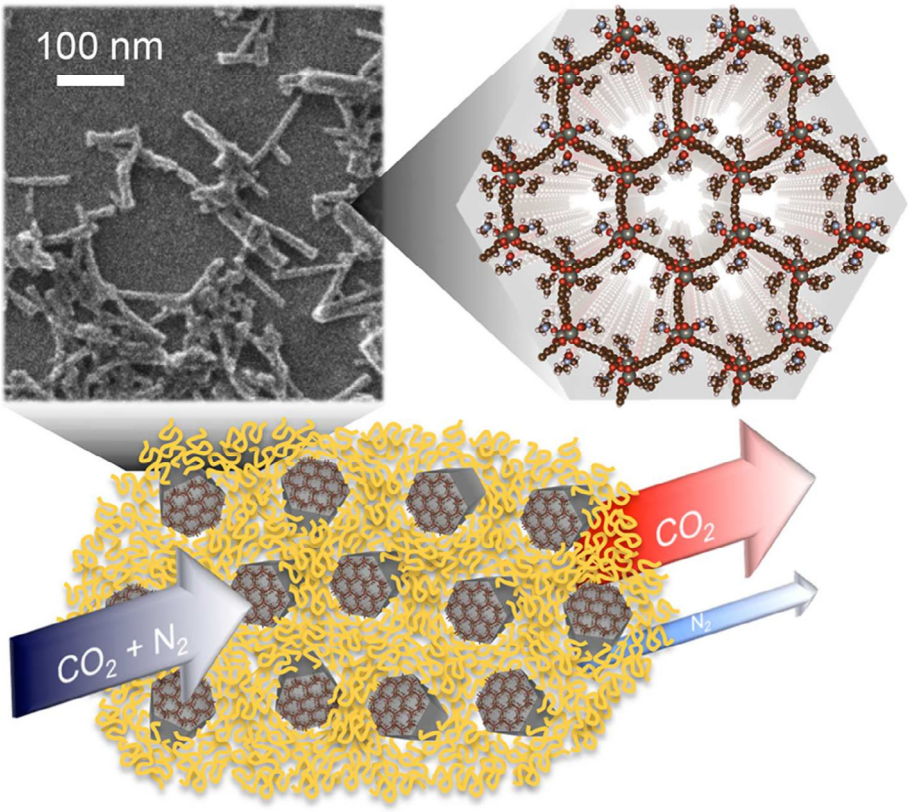

Fig. 22. (a) Schematic of mmen-Mg_2(dobpdc) nanorods in a mixed matrix membrane with high permeability and selectivity for CO_2/N_2 separation. Reproduced from ref. 205 with permission from the American Chemical Society, copyright 2017.

7. Conclusions and perspectives

In this review, we summarized recent advances in general synthetic strategies to obtain nanoMOFs with uniform size and good monodispersity as well as the MOF-based 1-D nanomaterials. Obviously, this work is extremely challenging. Currently, there has been yet one method to prepare uniform nanoMOFs with all kinds of structures. By carefully segregating the nucleation and growth process during the synthesis of MOFs, solvothermal and microemulsion methods offer the greatest possibility. However, due to the diversity of MOFs and the complexity of their growth process, more efforts should be made in the future.

As for the applications of nanoMOFs, they are currently most widely used in the field of biomedicine thanks to their proper sizes, chemical versatility, good biocompatibility, tunable structure, appropriate and physiological stability, etc. Some nanoMOF materials with therapeutic functions, such as porphyrin-based MOFs, can not only directly act as therapeutic agents, but also can be used as drug carriers to load anticancer drugs, so as to achieve synergistically enhanced treatment of tumours. However, the study on

nanoMOF materials for clinical application is still in its infancy at present. NanoMOF therapeutics with high biological safety is urgently needed in the future. In the fields of catalysis, nanoMOFs possessing very high external surface area, coupled with the shorter diffusion pathway of reactants and products, are highly desired and beneficial to catalytic efficiency. In addition, past investigations have witnessed the superiority of metal nanoparticles/MOF composites for improved catalytic performance. However, the nano-sizes, uniformity and monodispersity of MOFs in these composites have been largely ignored so far. We propose to use uniform and monodispersed nanoMOF materials to load tiny metal nanoparticles, and the resulting catalysts might have great potential for further improvement in catalytic performance. In addition, nanoMOF materials provide great adaptability/compatibility with other components, which greatly facilitates the integration of their respective advantages, thereby improving the catalysis-, energy- and membrane separation-related performance of resultant composites.

Obviously, more applications will benefit from the intrinsic properties of smaller microcrystalline MOFs. Therefore, it is important to continue to advance the size-controlled synthesis of nano-MOFs. Many recent findings have confirmed the excellent performance of nanoMOFs in diverse fields, in addition to the examples we discussed above. With continued efforts of scientists and development of the nanoMOF field, we expect to see more rational and general approaches to manipulate the controlled synthesis of nano-sized MOFs, and thus to serve for enhanced performances. We believe many exciting results related to nanoMOFs will be reported in the near future.

Declaration of Competing Interest

The authors declare that they have no known competing financial interests or personal relationships that could have appeared to influence the work reported in this paper.

Acknowledgments

This work was supported by the National Science Fund for Distinguished Young Scholars (No. 21725101, 21825106), the NSFC (21673213, 21871244, 21701160, 21521001 and 21671175), the Program for Science & Technology Innovation Talents in Universities of Henan Province (164100510005), the Program for Innovative Research Team (in Science and Technology) in Universities of Henan Province (19IRTSTHN022) and Zhengzhou University.

Appendix A. Supplementary data

Supplementary data to this article can be found online at https://doi.org/10.1016/j.ccr.2020.213366.

References

[1] H. Gleiter, Acta Mater. 48 (2000) 1–29.
[2] L. Zhang, M. Zhou, A. Wang, T. Zhang, Chem. Rev. 120 (2020) 683–733.
[3] F. Yang, D. Deng, X. Pan, Q. Fu, X. Bao, Natl. Sci. Rev. 2 (2015) 183–201.
[4] B. Li, H.M. Wen, Y. Cui, W. Zhou, G. Qian, B. Chen, Adv. Mater. 28 (2016) 8819–8860.
[5] J.R. Long, O.M. Yaghi, Chem. Soc. Rev. 38 (2009) 1213–1214.
[6] H.-C. Zhou, J.R. Long, O.M. Yaghi, Chem. Rev. 112 (2012) 673–674.
[7] H. Furukawa, K.E. Cordova, M. O'Keeffe, O.M. Yaghi, Science 341 (2013) 1230444.
[8] L. Jiao, J.Y.R. Seow, W.S. Skinner, Z.U. Wang, H.-L. Jiang, Mater. Today 27 (2019) 43–68.
[9] R.-W. Huang, Y.-S. Wei, X.-Y. Dong, X.-H. Wu, C.-X. Du, S.-Q. Zang, T.C. Mak, Nat. Chem. 9 (2017) 689.
[10] D. Li, H.-Q. Xu, L. Jiao, H.-L. Jiang, EnergyChem 1 (2019) 100005.
[11] M. Ding, X. Cai, H.-L. Jiang, Chem. Sci. 10 (2019) 10209–10230.
[12] Z. Liang, R. Zhao, T. Qiu, R. Zou, Q. Xu, EnergyChem 1 (2019) 100001.
[13] P. Li, F.-F. Cheng, W.-W. Xiong, Q. Zhang, Inorg. Chem. Front. 5 (2018) 2693–2708.
[14] J. Zhao, X. Liu, Y. Wu, D.-S. Li, Q. Zhang, Coord. Chem. Rev. 391 (2019) 30–43.
[15] J. Lee, O.K. Farha, J. Roberts, K.A. Scheidt, S.T. Nguyen, J.T. Hupp, Chem. Soc. Rev. 38 (2009) 1450–1459.
[16] A. Corma, H. García, F.X. Llabrés i Xamena, Chem. Rev. 110 (2010) 4606–4655.
[17] L. Jiao, Y. Wang, H.L. Jiang, Q. Xu, Adv. Mater. 30 (2018) 1703663.
[18] J. Liu, L. Chen, H. Cui, J. Zhang, L. Zhang, C.-Y. Su, Chem. Soc. Rev. 43 (2014) 6011–6061.
[19] Y.-B. Huang, J. Liang, X.-S. Wang, R. Cao, Chem. Soc. Rev. 46 (2017) 126–157.
[20] Q. Yang, Q. Xu, H.-L. Jiang, Chem. Soc. Rev. 46 (2017) 4774–4808.
[21] M. Zhao, S. Ou, C.-D. Wu, Acc. Chem. Res. 47 (2014) 1199–1207.
[22] L. Jiao, H.-L. Jiang, Chem 5 (2019) 786–804.
[23] A. Karmakar, A.J. Pombeiro, Coord. Chem. Rev. 395 (2019) 86–129.
[24] G. Li, S. Zhao, Y. Zhang, Z. Tang, Adv. Mater. 30 (2018) 1800702.
[25] Y.-H. Luo, L.-Z. Dong, J. Liu, S.-L. Li, Y.-Q. Lan, Coord. Chem. Rev. 390 (2019) 86–126.
[26] Y.-T. Liao, B.M. Matsagar, K.C.-W. Wu, ACS Sustainable Chem. Eng. 6 (2018) 13628–13643.
[27] Y.V. Kaneti, S. Dutta, M.S. Hossain, M.J. Shiddiky, K.L. Tung, F.K. Shieh, C.K. Tsung, K.C.W. Wu, Y. Yamauchi, Adv. Mater. 29 (2017) 1700213.
[28] Y.-P. Wu, X.-Q. Wu, J.-F. Wang, J. Zhao, W.-W. Dong, D.-S. Li, Q.-C. Zhang, Cryst. Growth Des. 16 (2016) 2309–2316.
[29] X. Zhao, Y. Wang, D.-S. Li, X. Bu, P. Feng, Adv. Mater. 30 (2018) 1705189.
[30] S. Krause, V. Bon, I. Senkovska, U. Stoeck, D. Wallacher, D.M. Többens, S. Zander, R.S. Pillai, G. Maurin, F.-X. Coudert, S. Kaskel, Nature 532 (2016) 348–352.
[31] M. Ding, R.W. Flaig, H.-L. Jiang, O.M. Yaghi, Chem. Soc. Rev. 48 (2019) 2783–2828.
[32] J.E. Bachman, Z.P. Smith, T. Li, T. Xu, J.R. Long, Nat. Mater. 15 (2016) 845.
[33] J.-R. Li, Y. Ma, M.C. McCarthy, J. Sculley, J. Yu, H.-K. Jeong, P.B. Balbuena, H.-C. Zhou, Coord. Chem. Rev. 255 (2011) 1791–1823.
[34] D.-D. Zhou, X.-W. Zhang, Z.-W. Mo, Y.-Z. Xu, X.-Y. Tian, Y. Li, X.-M. Chen, J.-P. Zhang, EnergyChem 1 (2019) 100016.
[35] H. Li, L. Li, R.-B. Lin, W. Zhou, S. Xiang, B. Chen, Z. Zhang, EnergyChem 1 (2019) 100006.
[36] Y. Wang, D. Zhao, Cryst. Growth Des. 17 (2017) 2291–2308.
[37] P. Horcajada, R. Gref, T. Baati, P.K. Allan, G. Maurin, P. Couvreur, G. Ferey, R.E. Morris, C. Serre, Chem. Rev. 112 (2011) 1232–1268.
[38] K. Lu, T. Aung, N. Guo, R. Weichselbaum, W. Lin, Adv. Mater. 30 (2018) 1707634.
[39] I.A. Lázaro, R.S. Forgan, Coord. Chem. Rev. 380 (2019) 230–259.
[40] G. Lan, K. Ni, W. Lin, Coord. Chem. Rev. 379 (2019) 65–81.
[41] M.X. Wu, Y.W. Yang, Adv. Mater. 29 (2017) 1606134.
[42] M. Lismont, L. Dreesen, S. Wuttke, Adv. Funct. Mater. 27 (2017) 1606314.
[43] W. Cai, C.-C. Chu, G. Liu, Y.-X.J. Wáng, Small 11 (2015) 4806–4822.
[44] F.-K. Shieh, S.-C. Wang, C.-I. Yen, C.-C. Wu, S. Dutta, L.-Y. Chou, J.V. Morabito, P. Hu, M.-H. Hsu, K.C.-W. Wu, J. Am. Chem. Soc. 137 (2015) 4276–4279.
[45] S. Dutta, J. Kim, P.H. Hsieh, Y.S. Hsu, Y.V. Kaneti, F.K. Shieh, Y. Yamauchi, K.C. W. Wu, Small Methods 3 (2019) 1900213.
[46] F.Y. Yi, D. Chen, M.K. Wu, L. Han, H.-L. Jiang, ChemPlusChem 81 (2016) 675–690.
[47] J. He, J. Xu, J. Yin, N. Li, X.-H. Bu, Sci. China Mater. 62 (2019) 1655–1678.
[48] L.E. Kreno, K. Leong, O.K. Farha, M. Allendorf, R.P. Van Duyne, J.T. Hupp, Chem. Rev. 112 (2011) 1105–1125.
[49] Z. Hu, B.J. Deibert, J. Li, Chem. Soc. Rev. 43 (2014) 5815–5840.
[50] J. Rocha, L.D. Carlos, F.A.A. Paz, D. Ananias, Chem. Soc. Rev. 40 (2011) 926–940.
[51] W.P. Lustig, S. Mukherjee, N.D. Rudd, A.V. Desai, J. Li, S.K. Ghosh, Chem. Soc. Rev. 46 (2017) 3242–3285.
[52] Y. Cui, B. Chen, G. Qian, Coord. Chem. Rev. 273 (2014) 76–86.
[53] G.W. Xu, Y.P. Wu, W.W. Dong, J. Zhao, X.Q. Wu, D.S. Li, Q. Zhang, Small 13 (2017) 1602996.
[54] Z.-S. Qin, W.-W. Dong, J. Zhao, Y.-P. Wu, Q. Zhang, D.-S. Li, Inorg. Chem. Front. 5 (2018) 120–126.
[55] X. Ma, Y. Chai, P. Li, B. Wang, Acc. Chem. Res. 52 (2019) 1461–1470.
[56] F.Y. Yi, R. Zhang, H. Wang, L.F. Chen, L. Han, H.-L. Jiang, Q. Xu, Small Methods 1 (2017) 1700187.
[57] K.-B. Wang, Q. Xun, Q. Zhang, EnergyChem 2 (2020) 100025.
[58] H. Wang, Q.-L. Zhu, R. Zou, Q. Xu, Chem 2 (2017) 52–80.
[59] C.A. Downes, S.C. Marinescu, ChemSusChem 10 (2017) 4374–4392.
[60] X. Li, X. Yang, H. Xue, H. Pang, Q. Xu, EnergyChem 2 (2020) 100027.
[61] L. Zhang, H. Liu, W. Shi, P. Cheng, Coord. Chem. Rev. 388 (2019) 293–309.
[62] Z. Wu, J. Xie, Z.J. Xu, S. Zhang, Q. Zhang, J. Mater. Chem. A 7 (2019) 4259–4290.
[63] J.Y. Kim, H. Oh, H.R. Moon, Adv. Mater. 31 (2019) 1805293.
[64] P. Ramaswamy, N.E. Wong, G.K. Shimizu, Chem. Soc. Rev. 43 (2014) 5913–5932.
[65] P.-L. Wang, L.-H. Xie, E.A. Joseph, J.-R. Li, X.-O. Su, H.-C. Zhou, Chem. Rev. 119 (2019) 10638–10690.
[66] L. Wang, H. Xu, J. Gao, J. Yao, Q. Zhang, Coord. Chem. Rev. 398 (2019) 213016.
[67] A. Carne, C. Carbonell, I. Imaz, D. Maspoch, Chem. Soc. Rev. 40 (2011) 291–305.
[68] X. Xiao, L. Zou, H. Pang, Q. Xu, Chem. Soc. Rev. 49 (2020) 301–331.

[69] S. Wang, C.M. McGuirk, A. d'Aquino, J.A. Mason, C.A. Mirkin, Adv. Mater. 30 (2018) 1800202.
[70] E.A. Flügel, A. Ranft, F. Haase, B.V. Lotsch, J. Mater. Chem. 22 (2012) 10119–10133.
[71] C.R. Marshall, S.A. Staudhammer, C.K. Brozek, Chem. Sci. 10 (2019) 9396–9408.
[72] M.B. Majewski, H. Noh, T. Islamoglu, O.K. Farha, J. Mater. Chem. A 6 (2018) 7338–7350.
[73] Y.-Z. Li, Z.-H. Fu, G. Xu, Coord. Chem. Rev. 388 (2019) 79–106.
[74] M. Zhao, Y. Huang, Y. Peng, Z. Huang, Q. Ma, H. Zhang, Chem. Soc. Rev. 47 (2018) 6267–6295.
[75] M. Zhao, Q. Lu, Q. Ma, H. Zhang, Small Methods 1 (2017) 1600030.
[76] N.T.K. Thanh, N. Maclean, S. Mahiddine, Chem. Rev. 114 (2014) 7610–7630.
[77] M. Sindoro, N. Yanai, A.-Y. Jee, S. Granick, Acc. Chem. Res. 47 (2014) 459–469.
[78] N. Stock, S. Biswas, Chem. Rev. 112 (2012) 933–969.
[79] T. Chalati, P. Horcajada, R. Gref, P. Couvreur, C. Serre, J. Mater. Chem. 21 (2011) 2220–2227.
[80] P. Horcajada, C. Serre, D. Grosso, C. Boissiere, S. Perruchas, C. Sanchez, G. Férey, Adv. Mater. 21 (2009) 1931–1935.
[81] S. Hermes, T. Witte, T. Hikov, D. Zacher, S. Bahnmüller, G. Langstein, K. Huber, R.A. Fischer, J. Am. Chem. Soc. 129 (2007) 5324–5325.
[82] J. Cravillon, S. Münzer, S.-J. Lohmeier, A. Feldhoff, K. Huber, M. Wiebcke, Chem. Mater. 21 (2009) 1410–1412.
[83] F.K. Shieh, S.C. Wang, S.Y. Leo, K.C.W. Wu, Chem. Eur. J. 19 (2013) 11139–11142.
[84] T. Tsuruoka, S. Furukawa, Y. Takashima, K. Yoshida, S. Isoda, S. Kitagawa, Angew. Chem. Int. Ed. 48 (2009) 4739–4743.
[85] T. He, X. Xu, B. Ni, H. Wang, Y. Long, W. Hu, X. Wang, Nanoscale 9 (2017) 19209–19215.
[86] S. Ayala, K.C. Bentz, S.M. Cohen, Chem. Sci. 10 (2019) 1746–1753.
[87] R. Mejia-Ariza, J. Huskens, J. Mater. Chem. B 4 (2016) 1108–1115.
[88] T. Uemura, S. Kitagawa, J. Am. Chem. Soc. 125 (2003) 7814–7815.
[89] T. Uemura, Y. Hoshino, S. Kitagawa, K. Yoshida, S. Isoda, Chem. Mater. 18 (2006) 992–995.
[90] X. Cai, J. Lin, M. Pang, Cryst. Growth Des. 16 (2016) 3565–3568.
[91] Y. Gu, M. Huang, W. Zhang, M.A. Pearson, J.A. Johnson, Angew. Chem. Int. Ed. 58 (2019) 16676–16681.
[92] X. Lan, N. Huang, J. Wang, T. Wang, Chem. Commun. 54 (2018) 584–587.
[93] X.G. Wang, Q. Cheng, Y. Yu, X.Z. Zhang, Angew. Chem. Int. Ed. 57 (2018) 7836–7840.
[94] A.K. Ganguli, A. Ganguly, S. Vaidya, Chem. Soc. Rev. 39 (2010) 474–485.
[95] S. Vaucher, M. Li, S. Mann, Angew. Chem. Int. Ed. 39 (2000) 1793–1796.
[96] W.J. Rieter, K.M. Taylor, H. An, W. Lin, W. Lin, J. Am. Chem. Soc. 128 (2006) 9024–9025.
[97] K.M. Taylor, W.J. Rieter, W. Lin, J. Am. Chem. Soc. 130 (2008) 14358–14359.
[98] X. Cai, Z. Xie, M. Pang, J. Lin, Cryst. Growth Des. 19 (2019) 556–561.
[99] X. Cai, X. Deng, Z. Xie, Y. Shi, M. Pang, J. Lin, Chem. Eng. J. 358 (2019) 369–378.
[100] X. Cai, B. Liu, M. Pang, J. Lin, Dalton Trans. 47 (2018) 16329–16336.
[101] W.H. Li, K. Ding, H.R. Tian, M.S. Yao, B. Nath, W.H. Deng, Y. Wang, G. Xu, Adv. Funct. Mater. 27 (2017) 1702067.
[102] W.-H. Li, J. Lv, Q. Li, J. Xie, N. Ogiwara, Y. Huang, H. Jiang, H. Kitagawa, G. Xu, Y. Wang, J. Mater. Chem. A 7 (2019) 10431–10438.
[103] M.-S. Yao, L.-A. Cao, Y.-X. Tang, G.-E. Wang, R.-H. Liu, P.N. Kumar, G.-D. Wu, W.-H. Deng, W.-J. Hong, G. Xu, J. Mater. Chem. A 7 (2019) 18397–18403.
[104] M.S. Yao, W.X. Tang, G.E. Wang, B. Nath, G. Xu, Adv. Mater. 28 (2016) 5229–5234.
[105] R. Ostermann, J. Cravillon, C. Weidmann, M. Wiebcke, B.M. Smarsly, Chem. Commun. 47 (2011) 442–444.
[106] W. Zhang, Z.-Y. Wu, H.-L. Jiang, S.-H. Yu, J. Am. Chem. Soc. 136 (2014) 14385–14388.
[107] C.-L. Zhang, B.-R. Lu, F.-H. Cao, Z.-Y. Wu, W. Zhang, H.-P. Cong, S.-H. Yu, Nano Energy 55 (2019) 226–233.
[108] Y.Z. Chen, C. Wang, Z.Y. Wu, Y. Xiong, Q. Xu, S.H. Yu, H.L. Jiang, Adv. Mater. 27 (2015) 5010–5016.
[109] J. Zhao, D.T. Lee, R.W. Yaga, M.G. Hall, H.F. Barton, I.R. Woodward, C.J. Oldham, H.J. Walls, G.W. Peterson, G.N. Parsons, Angew. Chem. Int. Ed. 55 (2016) 13224–13228.
[110] W. Huan, M. Xing, C. Cheng, J. Li, ACS Sustainable Chem. Eng. 7 (2019) 2245–2254.
[111] Y. Liu, Y. Zhao, X. Chen, Theranostics 9 (2019) 3122.
[112] C. He, D. Liu, W. Lin, Chem. Rev. 115 (2015) 11079–11108.
[113] P. Horcajada, R. Gref, T. Baati, P.K. Allan, G. Maurin, P. Couvreur, G. Férey, R.E. Morris, C. Serre, Chem. Rev. 112 (2012) 1232–1268.
[114] T. Simon-Yarza, A. Mielcarek, P. Couvreur, C. Serre, Adv. Mater. 30 (2018) 1707365.
[115] M. Giménez-Marqués, T. Hidalgo, C. Serre, P. Horcajada, Coord. Chem. Rev. 307 (2016) 342–360.
[116] P. Horcajada, T. Chalati, C. Serre, B. Gillet, C. Sebrie, T. Baati, J.F. Eubank, D. Heurtaux, P. Clayette, C. Kreuz, J.-S. Chang, Y.K. Hwang, V. Marsaud, P.-N. Bories, L. Cynober, S. Gil, G. Férey, P. Couvreur, R. Gref, Nat. Mater. 9 (2010) 172.
[117] C. He, K. Lu, D. Liu, W. Lin, J. Am. Chem. Soc. 136 (2014) 5181–5184.
[118] H. Zheng, Y. Zhang, L. Liu, W. Wan, P. Guo, A.M. Nyström, X. Zou, J. Am. Chem. Soc. 138 (2016) 962–968.
[119] J. Park, Q. Jiang, D. Feng, L. Mao, H.-C. Zhou, J. Am. Chem. Soc. 138 (2016) 3518–3525.
[120] K. Lu, C. He, W. Lin, J. Am. Chem. Soc. 136 (2014) 16712–16715.
[121] K. Lu, C. He, W. Lin, J. Am. Chem. Soc. 137 (2015) 7600–7603.
[122] J. Liu, Y. Yang, W. Zhu, X. Yi, Z. Dong, X. Xu, M. Chen, K. Yang, G. Lu, L. Jiang, Z. Liu, Biomaterials 97 (2016) 1–9.
[123] J. Park, D. Feng, S. Yuan, H.-C. Zhou, Angew. Chem. Int. Ed. 54 (2015) 430–435.
[124] L. Zhang, J. Lei, F. Ma, P. Ling, J. Liu, H. Ju, Chem. Commun. 51 (2015) 10831–10834.
[125] J. Park, Q. Jiang, D. Feng, H.-C. Zhou, Angew. Chem. Int. Ed. 55 (2016) 7188–7193.
[126] S.-S. Wan, J.-Y. Zeng, H. Cheng, X.-Z. Zhang, Biomaterials 185 (2018) 51–62.
[127] S.-Y. Li, H. Cheng, B.-R. Xie, W.-X. Qiu, J.-Y. Zeng, C.-X. Li, S.-S. Wan, L. Zhang, W.-L. Liu, X.-Z. Zhang, ACS Nano 11 (2017) 7006–7018.
[128] H.-S. Wang, Coord. Chem. Rev. 349 (2017) 139–155.
[129] C. Tian, L. Zhu, F. Lin, S.G. Boyes, A.C.S. Appl, Mater. Interfaces 7 (2015) 17765–17775.
[130] K.M. Taylor, A. Jin, W. Lin, Angew. Chem. Int. Ed. 47 (2008) 7722–7725.
[131] R. Nishiyabu, N. Hashimoto, T. Cho, K. Watanabe, T. Yasunaga, A. Endo, K. Kaneko, T. Niidome, M. Murata, C. Adachi, J. Am. Chem. Soc. 131 (2009) 2151–2158.
[132] M.D. Rowe, D.H. Thamm, S.L. Kraft, S.G. Boyes, Biomacromolecules 10 (2009) 983–993.
[133] L. Qin, Z.-Y. Sun, K. Cheng, S.-W. Liu, J.-X. Pang, L.-M. Xia, W.-H. Chen, Z. Cheng, J.-X. Chen, ACS Appl. Mater. Interfaces 9 (2017) 41378–41386.
[134] T. Kundu, S. Mitra, D. Diaz Diaz, R. Banerjee, ChemPlusChem 81 (2016) 728–732.
[135] D.R. Broome, M.S. Girguis, P.W. Baron, A.C. Cottrell, I. Kjellin, G.A. Kirk, Am. J. Roentgenol. 188 (2007) 586–592.
[136] L. Thunus, R. Lejeune, Coord. Chem. Rev. 184 (1999) 125–155.
[137] D. Liu, C. He, C. Poon, W. Lin, J. Mater. Chem. B 2 (2014) 8249–8255.
[138] G. Paul, Y. Prado, N. Dia, E. Riviere, S. Laurent, M. Roch, L. Vander Elst, R.N. Muller, L. Sancey, P. Perriat, Chem. Commun. 50 (2014) 6740–6743.
[139] M. He, Y. Chen, C. Tao, Q. Tian, L. An, J. Lin, Q. Tian, H. Yang, S. Yang, ACS Appl. Mater. Interfaces 11 (2019) 41946–41956.
[140] K. Brindle, Nat. Rev. Cancer 8 (2008) 94–107.
[141] K.E. deKrafft, Z. Xie, G. Cao, S. Tran, L. Ma, O.Z. Zhou, W. Lin, Angew. Chem. Int. Ed. 48 (2009) 9901–9904.
[142] K.E. deKrafft, W.S. Boyle, L.M. Burk, O.Z. Zhou, W. Lin, J. Mater. Chem. 22 (2012) 18139–18144.
[143] W. Zhang, Y. Hu, J. Ge, H.-L. Jiang, S.-H. Yu, J. Am. Chem. Soc. 136 (2014) 16978–16981.
[144] W.J. Rieter, K.M. Pott, K.M. Taylor, W. Lin, J. Am. Chem. Soc. 130 (2008) 11584–11585.
[145] T. Baati, L. Njim, F. Neffati, A. Kerkeni, M. Bouttemi, R. Gref, M.F. Najjar, A. Zakhama, P. Couvreur, C. Serre, P. Horcajada, Chem. Sci. 4 (2013) 1597–1607.
[146] S. Peng, B. Bie, Y. Sun, M. Liu, H. Cong, W. Zhou, Y. Xia, H. Tang, H. Deng, X. Zhou, Nat. Commun. 9 (2018) 1293.
[147] J. Zhuang, C.-H. Kuo, L.-Y. Chou, D.-Y. Liu, E. Weerapana, C.-K. Tsung, ACS Nano 8 (2014) 2812–2819.
[148] N.L. Torad, M. Hu, Y. Kamachi, K. Takai, M. Imura, M. Naito, Y. Yamauchi, Chem. Commun. 49 (2013) 2521–2523.
[149] Y. Pan, D. Heryadi, F. Zhou, L. Zhao, G. Lestari, H. Su, Z. Lai, CrystEngComm 13 (2011) 6937–6940.
[150] Y. Pan, Y. Liu, G. Zeng, L. Zhao, Z. Lai, Chem. Commun. 47 (2011) 2071–2073.
[151] L. Gao, Q. Chen, T. Gong, J. Liu, C. Li, Nanoscale 11 (2019) 21030–21045.
[152] L. Su, Q. Wu, L. Tan, Z. Huang, C. Fu, X. Ren, N. Xia, Z. Chen, X. Ma, X. Lan, A.C.S. Appl, Mater. Interfaces 11 (2019) 10520–10531.
[153] J.-C. Yang, Y. Shang, Y.-H. Li, Y. Cui, X.-B. Yin, Chem. Sci. 9 (2018) 7210–7217.
[154] W. Zhang, S. Li, X. Liu, C. Yang, N. Hu, L. Dou, B. Zhao, Q. Zhang, Y. Suo, J. Wang, Adv. Funct. Mater. 28 (2018) 1706375.
[155] Y. Liu, W. Zhen, L. Jin, S. Zhang, G. Sun, T. Zhang, X. Xu, S. Song, Y. Wang, J. Liu, ACS Nano 12 (2018) 4886–4893.
[156] W. Zhou, L. Wang, F. Li, W. Zhang, W. Huang, F. Huo, H. Xu, Adv. Funct. Mater. 27 (2017) 1605465.
[157] H. Zhang, Q. Li, R. Liu, X. Zhang, Z. Li, Y. Luan, Adv. Funct. Mater. 28 (2018) 1802830.
[158] Q. Wu, M. Niu, X. Chen, L. Tan, C. Fu, X. Ren, J. Ren, L. Li, K. Xu, H. Zhong, Biomaterials 162 (2018) 132–143.
[159] W. Jiang, H. Zhang, J. Wu, G. Zhai, Z. Li, Y. Luan, S. Garg, ACS Appl. Mater. Interfaces 10 (2018) 34513–34523.
[160] Y. Li, J. Jin, D. Wang, J. Lv, K. Hou, Y. Liu, C. Chen, Z. Tang, Nano Research 11 (2018) 3294–3305.
[161] H. Zhang, C. Hao, A. Qu, M. Sun, L. Xu, C. Xu, H. Kuang, Adv. Funct. Mater. 28 (2018) 1805320.
[162] W.-H. Chen, G.-F. Luo, M. Vázquez-González, R.m. Cazelles, Y.S. Sohn, R. Nechushtai, Y. Mandel, I. Willner, ACS Nano 12 (2018) 7538–7545.
[163] W.-H. Chen, M. Vázquez-González, A. Zoabi, R. Abu-Reziq, I. Willner, Nat. Catal. 1 (2018) 689–695.
[164] D. Feng, Z.-Y. Gu, J.-R. Li, H.-L. Jiang, Z. Wei, H.-C. Zhou, Angew. Chem. Int. Ed. 51 (2012) 10307–10310.
[165] H.-L. Jiang, D. Feng, K. Wang, Z.-Y. Gu, Z. Wei, Y.-P. Chen, H.-C. Zhou, J. Am. Chem. Soc. 135 (2013) 13934–13938.
[166] D. Feng, Z.-Y. Gu, Y.-P. Chen, J. Park, Z. Wei, Y. Sun, M. Bosch, S. Yuan, H.-C. Zhou, J. Am. Chem. Soc. 136 (2014) 17714–17717.
[167] J.-L. Kan, Y. Jiang, A. Xue, Y.-H. Yu, Q. Wang, Y. Zhou, Y.-B. Dong, Inorg. Chem. 57 (2018) 5420–5428.

[168] J.Y. Zeng, M.K. Zhang, M.Y. Peng, D. Gong, X.Z. Zhang, Adv. Funct. Mater. 28 (2018) 1705451.
[169] Z. Zhou, A. Chan, Z. Wang, X. Huang, G. Yu, O. Jacobson, S. Wang, Y. Liu, L. Shan, Y. Dai, Angew. Chem. Int. Ed. 57 (2018) 8463–8467.
[170] T.-T. Jia, G. Yang, S.-J. Mo, Z.-Y. Wang, B.-J. Li, W. Ma, Y.-X. Guo, X. Chen, X. Zhao, J.-Q. Liu, ACS Nano 13 (2019) 8320–8328.
[171] X.D. Zhang, Z. Luo, J. Chen, X. Shen, S. Song, Y. Sun, S. Fan, F. Fan, D.T. Leong, J. Xie, Adv. Mater. 26 (2014) 4565–4568.
[172] X.D. Zhang, J. Chen, Z. Luo, D. Wu, X. Shen, S.S. Song, Y.M. Sun, P.X. Liu, J. Zhao, S. Huo, S. Fan, F. Fan, X.-J. Liang, J. Xie, Adv. Health. Mater. 3 (2014) 133–141.
[173] G. Song, L. Cheng, Y. Chao, K. Yang, Z. Liu, Adv. Mater. 29 (2017) 1700996.
[174] K. Ni, G. Lan, S.S. Veroneau, X. Duan, Y. Song, W. Lin, Nat. Commun. 9 (2018) 4321.
[175] G. Lan, K. Ni, S.S. Veroneau, T. Luo, E. You, W. Lin, J. Am. Chem. Soc. 141 (2019) 6859–6863.
[176] W. Liu, Y.M. Wang, Y.H. Li, S.J. Cai, X.B. Yin, X.W. He, Y.K. Zhang, Small 13 (2017) 1603459.
[177] Y. Zhang, F. Wang, C. Liu, Z. Wang, L. Kang, Y. Huang, K. Dong, J. Ren, X. Qu, ACS Nano 12 (2018) 651–661.
[178] G. Lan, K. Ni, S.S. Veroneau, X. Feng, G.T. Nash, T. Luo, Z. Xu, W. Lin, J. Am. Chem. Soc. 141 (2019) 4204–4208.
[179] X. Cai, Z. Xie, B. Ding, S. Shao, S. Liang, M. Pang, J. Lin, Adv. Sci. 6 (2019) 1900848.
[180] W. Wang, L. Wang, Y. Li, S. Liu, Z. Xie, X. Jing, Adv. Mater. 28 (2016) 9320–9325.
[181] X. Zheng, L. Wang, M. Liu, P. Lei, F. Liu, Z. Xie, Chem. Mater. 30 (2018) 6867–6876.
[182] S.M.J. Rogge, A. Bavykina, J. Hajek, H. Garcia, A.I. Olivos-Suarez, A. Sepúlveda-Escribano, A. Vimont, G. Clet, P. Bazin, F. Kapteijn, M. Daturi, E.V. Ramos-Fernandez, F.X. Llabrés i Xamena, V. Van Speybroeck, J. Gascon Chem. Soc. Rev. 46 (2017) 3134–3184.
[183] G. Cai, M. Ding, Q. Wu, H.-L. Jiang, Natl. Sci. Rev. 7 (2020) 37–45.
[184] T. Kiyonaga, M. Higuchi, T. Kajiwara, Y. Takashima, J. Duan, K. Nagashima, S. Kitagawa, Chem. Commun. 51 (2015) 2728–2730.
[185] P. Li, R.C. Klet, S.-Y. Moon, T.C. Wang, P. Deria, A.W. Peters, B.M. Klahr, H.-J. Park, S.S. Al-Juaid, J.T. Hupp, O.K. Farha, Chem. Commun. 51 (2015) 10925–10928.
[186] P. Li, S.-Y. Moon, M.A. Guelta, L. Lin, D.A. Gómez-Gualdrón, R.Q. Snurr, S.P. Harvey, J.T. Hupp, O.K. Farha, ACS Nano 10 (2016) 9174–9182.
[187] Y. Qi, Y. Luan, J. Yu, X. Peng, G. Wang, Chem. Eur. J. 21 (2015) 1589–1597.
[188] H.-C. Lee, T. Heil, J.-K. Sun, B.V.K.J. Schmidt, Mater. Horiz. 6 (2019) 802–809.
[189] A.L. Semrau, P.M. Stanley, A. Urstoeger, M. Schuster, M. Cokoja, R.A. Fischer, ACS Catal. 10 (2020) 3203–3211.
[190] Q. Yang, Q. Xu, S.H. Yu, H.L. Jiang, Angew. Chem. Int. Ed. 55 (2016) 3685–3689.
[191] T.-Y. Chen, Y.-J. Huang, C.-T. Li, C.-W. Kung, R. Vittal, K.-C. Ho, Nano Energy 32 (2017) 19–27.
[192] L. Wang, X. Feng, L. Ren, Q. Piao, J. Zhong, Y. Wang, H. Li, Y. Chen, B. Wang, J. Am. Chem. Soc. 137 (2015) 4920–4923.
[193] H.-N. Wang, M. Zhang, A.-M. Zhang, F.-C. Shen, X.-K. Wang, S.-N. Sun, Y.-J. Chen, Y.-Q. Lan, ACS Appl. Mater. Interfaces 10 (2018) 32265–32270.
[194] J.D. Xiao, Q. Shang, Y. Xiong, Q. Zhang, Y. Luo, S.H. Yu, H.L. Jiang, Angew. Chem. Int. Ed. 55 (2016) 9389–9393.
[195] P. Wen, P. Gong, J. Sun, J. Wang, S. Yang, J. Mater. Chem. A 3 (2015) 13874–13883.
[196] Q. Wang, Q. Wang, B. Xu, F. Gao, F. Gao, C. Zhao, Electrochim. Acta 281 (2018) 69–77.
[197] Y. Mao, H. Huang, W. Cao, J. Li, L. Sun, X. Jin, X. Peng, Chem. Commun. 49 (2013) 5666–5668.
[198] Y.-N. Wu, F. Li, H. Liu, W. Zhu, M. Teng, Y. Jiang, W. Li, D. Xu, D. He, P. Hannam, J. Mater. Chem. 22 (2012) 16971–16978.
[199] Y. Zhang, X. Feng, S. Yuan, J. Zhou, B. Wang, Inorg. Chem. Front. 3 (2016) 896–909.
[200] S. Qiu, M. Xue, G. Zhu, Chem. Soc. Rev. 43 (2014) 6116–6140.
[201] B.S. Ghanem, R. Swaidan, E. Litwiller, I. Pinnau, Adv. Mater. 26 (2014) 3688–3692.
[202] Z. Wang, D. Wang, S. Zhang, L. Hu, J. Jin, Adv. Mater. 28 (2016) 3399–3405.
[203] C. Kong, H. Du, L. Chen, B. Chen, Energy Environ. Sci. 10 (2017) 1812–1819.
[204] B. Ghalei, K. Sakurai, Y. Kinoshita, K. Wakimoto, Ali P. Isfahani, Q. Song, K. Doitomi, S. Furukawa, H. Hirao, H. Kusuda, S. Kitagawa, E. Sivaniah, Nat. Energy 2 (2017) 17086.
[205] L. Maserati, S.M. Meckler, J.E. Bachman, J.R. Long, B.A. Helms, Nano Lett. 17 (2017) 6828–6832.